Vertical escape tactics and movement potential of orthoconic cephalopods

David Joseph Peterman[1], Kathleen Anita Ritterbush[1]

[1] Department of Geology and Geophysics, University of Utah, Salt Lake City, Utah, USA

Corresponding Author:
David J. Peterman[1]
115, Salt Lake City, UT 84112, USA
Email address: David.Peterman@utah.edu

Abstract

Measuring locomotion tactics available to ancient sea animals can link functional morphology with evolution and ecology over geologic timescales. Externally-shelled cephalopods are particularly important for their central roles in marine trophic exchanges, but most fossil taxa lack sufficient modern analogues for comparison. In particular, phylogenetically diverse cephalopods produced orthoconic conchs (straight shells) repeatedly through time. Persistent re-evolution of this morphotype suggests that it possesses adaptive value. Practical lateral propulsion is ruled out as an adaptive driver among orthoconic cephalopods due to the stable, vertical orientations of taxa lacking sufficient counterweights. However, this constraint grants the possibility of rapid (or at least efficient) vertical propulsion. We experiment with this form of movement using 3D-printed models of *Baculites compressus*, weighted to mimic hydrostatic properties inferred by virtual models. Furthermore, model buoyancy was manipulated to impart simulated thrust within four independent scenarios (*Nautilus*-like cruising thrust; a similar thrust scaled by the mantle cavity of *Sepia*; sustained peak *Nautilus*-like thrust; and passive, slightly negative buoyancy). Each model was monitored underwater with two submerged cameras as they rose/fell over ~2 meters, and their kinematics were computed with 3D motion tracking. Our results demonstrate that orthocones require very low input thrust for high output in movement and velocity. With *Nautilus*-like peak thrust, the model reaches velocities of 1.2 m/s (2.1 body lengths per second) within one second starting from a static initial condition. While cephalopods with orthoconic conchs likely assumed a variety of life habits, these experiments illuminate some first-order constraints. Low hydrodynamic drag inferred by vertical displacement suggests that vertical migration would incur very low metabolic cost. While these cephalopods likely assumed low energy lifestyles day-to-day, they may have had a fighting chance to escape from larger, faster predators by performing quick, upward dodges. The current experiments suggest that orthocones sacrifice horizontal mobility and maneuverability in exchange for highly streamlined, vertically-stable, upwardly-motile conchs.

Introduction

A phylogenetically-diverse array of cephalopod mollusks produced straight conchs (orthocones) throughout geologic time, but their ecological contributions to marine systems are unclear. The evolutionary contexts of these animals are well documented: iconic spiral conchs of nautilids (extant) and ammonoids (extinct) are heavily-derived forms that follow early success by orthocone relatives (*Holland, 1987*). Orthoconic nautiloids were globally distributed and diverse in the Paleozoic, yielding hundreds of fossil genera (*Teichert et al., 1964*). A branch of orthocerid nautiloids gave rise to orthoconic bactritoids, and eventually to ammonoids (*Erben, 1966; Monnet, Klug, and De Baets, 2015*). Evolution of tightly-coiled ammonoid conchs in Early Devonian seas (by increased exogastric curvature; *Klug and Korn, 2004; Kröger and Mapes, 2007; Monnet, De Baets, and Klug, 2011*) may have radically increased horizontal mobility via hydrostatic and hydrodynamic features (aligning jet thrust to the animal's center of mass while simultaneously improving lateral streamlining; *Klug and Korn, 2004*). While coiled nautiloids evolved several times throughout the Paleozoic (e.g., mostly within Tarphycerida, Lituitida, Nautilida), the diversity and abundance of coiled ectocochleates relative to orthocones increased during this Devonian nekton revolution (*Klug et al., 2010*). Yet orthoconic nautiloid lineages commonly persisted until the Late Triassic and rarely into the Early Cretaceous (*Doguzhaeva, 1994*). Furthermore, orthoconic ammonoids repeatedly originated from planispiral ancestors through the Mesozoic (e.g., heteromorph species within Triassic Choristoceratidae, Jurassic Spiroceratidae, Late Jurassic/Early Cretaceous Bochianitidae, and Cretaceous Baculitidae; *Wiedmann, 1969; Wright, Callomon, and Howarth, 1996; Hoffmann et al., 2021*). The persistence and intermittent appearance of orthoconic forms suggests that this morphotype retained adaptive value, despite proliferation of planispiral conchs among these animals' contemporaries. However, the adaptive value, functional morphology, and ecology of orthoconic cephalopods are poorly understood. We aim to investigate these properties through hydrostatic and hydrodynamic analyses using the Cretaceous baculitid, *Baculites compressus* (North America, late Campanian), as a test case.

Hydrostatics of orthoconic cephalopods

Hydrostatic analyses suggest that orthoconic cephalopods assumed vertical orientations at rest (*Trueman, 1941; Westermann, 1977, 1996; Peterman et al., 2019; Peterman, Barton, and Yacobucci, 2019*). Mass would be anteriorly distributed near the body chamber (housing the animal's soft body) due to the overlying air-filled chambers (the phragmocone buoyancy apparatus). A static orientation occurs when the total center of mass is vertically aligned under the center of buoyancy (*Hoffmann et al., 2015*). When these centers are forced out of alignment, a restoring moment proportionate to their separation will act to return them to their static, equilibrium condition (*Peterman et al., 2019; Peterman et al., 2020a; Peterman et al., 2020b*). Mineral deposits (i.e., cameral and endosiphuncular deposits) common among some Paleozoic nautiloid species would have influenced hydrostatics in some way. These deposits are formed syn vivo (*Seuss et al., 2011; Pohl and Klug, 2018;* for contrasting views see *Mutvei, 2018*), very

80   disparate in structure (*Teichert, 1933; Flower, 1955a; Fischer and Teichert, 1969*), and help
81   characterize several higher taxa of nautiloids (*King and Evans, 2019*). Though diverse clades had
82   such mineral deposits in their shells, they have been generally regarded as counterweights that
83   facilitated more horizontal postures in the water column (*Schmidt, 1930; Flower, 1955b;*
84   *Westermann, 1977; Holland, 1987; Crick, 1988; Chamberlain, 1993; Barskov et al., 2008*).
85   However, recent studies suggest these counterweights may have altered restoring moments and
86   dynamic conch orientation, while the static orientation would likely remain near vertical
87   (*Peterman, Barton, and Yacobucci, 2019*). More detailed simulations are required to understand
88   the degree to which these structures reduce hydrostatic stability.
89   Hydrostatic and hydrodynamic relationships (*Peterman et al., 2019; Peterman, Barton,*
90   *and Yacobucci, 2019*) do not readily support interpretations of orthoconic cephalopods as swift
91   horizontal swimmers, akin to extant squid (*Tsujita and Westermann, 1988*). First, the source of
92   jet thrust (i.e., the hyponome) is aligned vertically with the centers of buoyancy and mass
93   (*Peterman et al., 2019*), supporting that thrust energy would most efficiently be transmitted into
94   upward vertical movement during jet propulsion. If thrust was applied in a horizontal direction,
95   much energy would be lost to rocking since the source of jet thrust is situated much lower than
96   these two hydrostatic centers (*Peterman et al., 2019*). Moreover, thrust perpendicular to the long
97   axis of the conch would not be sufficient to orient the animal horizontally (for taxa lacking
98   substantial counterweights; *Peterman et al., 2019*). These properties strongly constrained how
99   orthoconic cephalopods would have interacted with their surroundings, fed, and evaded
100 predators. The source of thrust relative to the mass distribution and vertically streamlined conch
101 suggest that orthocones were adapted for improved vertical movement potential, but at the
102 expense of horizontal mobility.
103
104 **Orthoconic cephalopod paleoecology**
105   Constraining likely locomotory functions for orthoconic cephalopods can lend context to
106 a very diverse range of lineages that flourished throughout the Paleozoic and Mesozoic, and are
107 known from nearly all marine paleoenvironments around the globe (*Kennedy and Cobban, 1976;*
108 *Wright, Callomon, and Howarth, 1996; Kröger and Zhang, 2009; Kröger, Servais, and Zhang,*
109 *2009*). Orthoconic nautiloids are generally regarded as vertical migrants of the water column
110 and/or demersal based on occurrence data, morphological characters, and taphonomic patterns
111 (*Kröger, Servais, and Zhang, 2009*). Species recovered from offshore sediments may have
112 migrated vertically through pelagic landscapes of varied photic and oxygen zones; whereas
113 species recovered from more coastal deposits may have remained in the neritic zone where
114 demersal feeding would be available (*Kröger, Servais, and Zhang, 2009*). This demersal lifestyle
115 of feeding on benthic fauna is traditionally interpreted for orthocones (*Frey, 1989; Brett and*
116 *Walker, 2002; Barskov et al., 2008; Kröger and Zhang, 2009*). The remarkable disparity of
117 orthocone conchs (especially siphuncular characteristics; *Fischer and Teichert, 1969; Barskov et*
118 *al., 2008*) suggests there were some fundamental and/or nuanced differences in their life habits.

119   Therefore, either vertical migration or primarily demersal lifestyles are not ruled out in the
120   appropriate settings.
121   Orthoconic ammonoids, in contrast, are generally found in neritic and epicontinental
122   settings (*Kennedy and Cobban, 1976; Wright, Callomon, and Howarth, 1996*). The depth range
123   of baculitid ammonoids was around 50-100 m based on isotopic analyses of well-preserved shell
124   material (*Fatherree, Harries, and Quinn, 1998; Lukeneder et al., 2010; Henderson and Price,*
125   *2012; Lukeneder, 2015; Sessa et al., 2015; Landman et al., 2018; Hoffmann et al., 2021*). A
126   demersal life habit is generally inferred from these analyses due to their isotopic similarity with
127   the benthos (*Landman et al., 2018; Ferguson et al., 2019; Hoffmann et al., 2021*). Isotopic
128   studies also suggest that some baculitids spent most of their lives at methane seeps, supporting a
129   somewhat sedentary lifestyle (*Landman et al., 2018; Rowe et al., 2020*). However, baculitid
130   associations with streamlined midwater swimmers, and occurrences in deposits lacking demersal
131   taxa, suggest that these species could cope with life higher in the water column as well (*Tsujita*
132   *and Westermann, 1998; Landman, Cobban, and Larson, 2012*).
133   Key observations remain that suggest horizontal (or subvertical) modes were adopted by
134   at least some species of orthoconic cephalopods. Life habit can be inferred from color patterns
135   preserved on the conch. While some orthocones had color patterns around the entire
136   circumference, others have patterns restricted to the dorsum, suggesting countershading in a
137   nonvertical orientation (*Packard, 1988; Westermann, 1998; Kröger, Servais, and Zhang, 2009;*
138   *Manda and Turek, 2015*). These orientations can be explained by resting the soft body on the
139   benthos (*Flower, 1955c*) or by the use of active locomotion. The former would require some
140   amount of negative buoyancy and would only provide useful camouflage from above, while the
141   latter would require sustained jet thrust of considerable magnitude in forms with lower
142   hydrostatic stability (i.e., those with cameral or endosiphuncular deposits; *Peterman, Barton, and*
143   *Yacobucci, 2019*). Contrasting hydrostatic interpretations, aperture-forward, horizontal
144   movement was inferred for the baculitid ammonoid, *Sciponoceras*, based on the adoral growth
145   direction of a cirripede attached to the venter (*Hauschke, Schöllmann, and Keupp, 2011*). Similar
146   growth orientations are observed for epizoans on some nautiloid orthocones as well (*Baird et al.,*
147   *1989*).
148   While a single mode of life should not be invoked for all orthoconic cephalopods, the
149   practical challenges faced during the animals' life can be constrained through empirical studies.
150   The model ammonoid, *Baculites compressus*, can provide valuable insight for the vertical
151   movement potential and kinematics of this hydrostatically-stable morphotype. The anatomy and
152   propulsive capabilities likely varied within and between ammonoid and nautiloid groups; a wide
153   range of experimental conditions allow broader interpretations for how this common conch
154   morphotype may have functioned. Orthocone conch size, ornamentation, curvature, whorl
155   section anatomy, body chamber proportion, and internal sculpture vary between clades; certain
156   physical properties, too, could progressively differ for taxa with higher disparity from our
157   investigated species. Therefore, we primarily limit our interpretations to orthoconic ammonoids
158   and morphologically-similar nautiloids without substantial conch curvature or internal

159   counterweights. The ease or difficulty in vertical movement, similar to the behavior observed in
160   extant nautilids (*Ward et al., 1984; Ward, 1987; O'Dor et al., 1993; Dunstan, Ward, and*
161   *Marshall, 2011*) is of interest. Furthermore, the conditions required to vertically dodge larger,
162   faster, predators with more speed-efficient modes of locomotion (undulatory vs jet propulsion;
163   *Wells and O'Dor, 1986; Anderson and Grosenbaugh, 2005; Neil and Askew, 2018*) are explored
164   with a range of predator analogues. An investigation of these capabilities can yield clues
165   regarding the adaptive value of this enigmatic morphotype and its iterative recurrence in the
166   fossil record.
167
168   ## Materials & Methods
169   Three-dimensional motion tracking was performed on physical models of *Baculites*
170   *compressus* in order to investigate various hydrodynamic properties of the orthocone
171   morphotype. These models were constructed from the virtual hydrostatic model of *Peterman et*
172   *al. (2019)* (Fig. 1A). The exterior portion of this model was isolated in Blender (*Blender Online*
173   *Community, 2017*), then a soft body more closely resembling the baculitid reconstruction of
174   *Klug, Riegraf, and Lehmann (2012)* was fabricated and affixed to the aperture using the same
175   software (Fig. 1B). The coiled embryonic shell (ammonitella) was ignored due to its very small
176   scale (~0.7 mm; *Landman, 1982*). Instead, the model tapers to a point approximately 0.7 mm in
177   diameter. The *Baculites compressus* model in the current study was designed to have positive or
178   negative buoyant forces that simulate movement in the vertical directions using similar methods
179   to *Peterman et al. (2021a)*. Each model in the current study was constructed at a size of 57 cm
180   (from the conch apex to distal ends of the arms). An external 3D model of *Baculites compressus*
181   is stored in the morphosource.org database (ark:/87602/m4/359359).
182
183   **Vertical movement scenarios**
184   Differences between the mass of water displaced and total model mass were computed to
185   equal the forces produced during movement under four different scenarios: (1) *Nautilus*-like
186   cruising thrust, (2) *Nautilus*-like cruising thrust scaled by the mantle cavity ratio of extant
187   cuttlefish, (3) sustained maximum *Nautilus*-like thrust, and (4) slightly negative buoyancy
188   similar to extant *Nautilus*. For Scenario 1, the thrust of 0.015 N required for a 73 g *Nautilus* to
189   overcome drag at its maximum velocity (*Chamberlain, 1987*) was scaled by the mass of the
190   water displaced by the current orthocone model (212.209 g) to yield a target thrust value of
191   0.0436 N. The mass of water displaced is equal to organismal mass, assuming a neutrally
192   buoyant condition. This *Nautilus*-like thrust was then scaled from the mantle cavity ratio of
193   *Nautilus* (0.15; *Wells and O'Dor, 1991*) to the mantle cavity ratio of *Sepia* (0.25; *Wells and*
194   *O'Dor, 1991*) yielding a target thrust of 0.0727 N for Scenario 2. The maximum propulsive
195   thrust for *Nautilus* is a function of body size (*Chamberlain, 1987*). For Scenario 3, this maximum
196   thrust was computed by substituting the mass of the *Baculites compressus* model (212.209 g)
197   into the following formula reported by *Chamberlain (1987)*:
198                         $$T_{max} = 0.0021(m) - 0.103 \qquad\qquad (1)$$

199 Where T_{max} is the maximum propulsive thrust in Newtons and m is the organismal mass in
200 grams.
201   The model for Scenario 4 was made slightly negatively buoyant with a similar magnitude
202 observed in extant *Nautilus*. *Ward and Martin (1978)* report residual masses (not relieved by
203 buoyancy) for several wild-caught *Nautilus*. Focusing on larger individuals from their study
204 (>300 g), the average residual mass was 1.76 g with an average total mass (including the soft
205 body, conch, and chamber liquid) of 676.6 g (~0.26% of their organismal mass is not relieved by
206 buoyancy). This corresponds to a residual mass of 0.552 g for the orthocone model. In order to
207 manage error, the model mass for this scenario was lowered by 1 g. The model was then made
208 neutrally buoyant by adding liquid into an anterior chamber with a syringe through a self-healing
209 rubber cap. Once the model no longer sank or rose for ~30 seconds, it was considered neutrally
210 buoyant. Then the residual mass of 0.5 g was added with water through the syringe to make the
211 model negatively buoyant according to the computed value. This negatively buoyant scenario
212 was chosen to assess the speed of descent for this vertically-streamlined morphotype, and basic
213 swimming capabilities (e.g., vertical migration, pouncing).
214   Each target buoyant force depends on the mass of the water displaced by the models,
215 which depends on density. Water density (1.000 g/cm^3) was computed with a calibrated 100 ml
216 pycnometer using water from where the motion tracking experiments were conducted (described
217 below). Water conditions including temperature (~28°C) and salinity were held constant (or
218 nearly so) for measurements and all experiments.
219
220 **Baculites compressus model construction**
221   Each model is composed of three parts (Fig. 1B); air-filled voids, PLA (polylactic acid)
222 plastic, and bismuth counterweights. Bismuth was chosen because of its high density, low
223 melting point, and softness. Since the virtual models of these components are only digital
224 volumes, their densities were determined with a calibrated 100 ml pycnometer to compute their
225 masses. Virtual models of the counterweights were placed anteriorly (within the arm crown) with
226 fixed positions and volumes for each model. After determining an appropriate counterweight
227 volume (and therefore mass) for each model, the volumes of the internal voids were adjusted to
228 yield the proper total mass for each model. The positions of the voids were iteratively altered to
229 maintain the same total model mass, while imparting the same hydrostatic stability index (0.505)
230 and apex-upward orientation inferred from the virtual hydrostatic model (*Peterman et al., 2019*).
231 The virtual models were considered finished when their hydrostatic stabilities and thrusts
232 matched their target values to the third and fourth decimal places, respectively.
233   Hydrostatic stability indices were computed from the total center of mass and the center
234 of buoyancy. The center of buoyancy was computed from the model of the exterior interface
235 (i.e., a model of the water displaced). This center and the centers of mass for each material of
236 unique density (air, water, PLA plastic, bismuth counterweight), were computed in MeshLab
237 (*Cignoni and Ranzuglia, 2014*). The total center of mass was computed with the following
238 formula:

239
$$M = \frac{\Sigma(D * m_o)}{\Sigma m_o} \qquad (2)$$

240 Where M is the total center of mass in a principal direction, D is the center of mass of a single
241 object in each principal direction, and m_o is the mass of any object of unique density. All
242 coordinates are measured relative to the same arbitrary datum placed at the center of the aperture.
243   The hydrostatic stability index (S_t) was computed from the following equation (after
244 Okamoto, 1996):

245
$$S_t = \frac{D_{BM}}{\sqrt[3]{V}} \qquad (3)$$

246 Where D_{BM} is the distance between the center of buoyancy (B) and the center of mass (M),
247 computed with the 3D theorem of Pythagoras. V is the organismal volume (equal to the volume
248 of water displaced).
249   The mass distribution of the PLA plastic required to impart the desired hydrostatic
250 stability index was computed with the following formula:

251
$$D_{PLA} = \frac{M(m_{PLA} + m_{Bi} + m_{air} + m_{water}) - (D_{Bi}m_{Bi}) - (D_{air}m_{air}) - (D_{water}m_{water})}{(m_{PLA})} \qquad (4)$$

252 Where D_{PLA} is the location of the PLA center of mass from the datum in each principle direction.
253 M is the total center of mass in a particular principle direction, m is the mass of a model
254 component, and D is the center of mass of each model component in a particular principle
255 direction. Subscripts denote each model component. Water is present only in the negatively
256 buoyant model (1 g).
257   After each virtual model was completed, they were 3D printed in a vertical orientation
258 with an Ultimaker S5 in four parts (in order to fit within the available print volume). Each part
259 contained a watertight void (Fig. 1B) that was sealed during 3D printing. The model parts were
260 all printed without support material due to their generally low overhang angles (<60°). Each of
261 the four parts were chemically welded together with dichloromethane. High heat silicone molds
262 of the counterweights were cast from 3D prints. The counterweights were cast form these molds
263 by heating bismuth in a casting ladle with a propane torch, and evenly pouring the molten
264 bismuth into the mold. The counterweights were further processed by using a metal file and
265 silicon carbide paper until the desired volume and mass was reached. The counterweight masses
266 slightly differed from their virtual counterparts (from 0.7% to 5% different) because they were
267 used to compensate for subtle differences between the virtual and actual masses of the 3D
268 printed parts. This modification minimized error of the target masses at the expense of error in
269 hydrostatic stabilities. The hydrostatic stability indices of the physical models were recomputed
270 with Equation 3, and all model components (aside from air) were weighed in grams to the third
271 decimal place in order to report error in stability and simulated thrust. Tracking points were
272 painted on the apex and the distal end of the arms for each final model (Fig. 1C) to monitor their
273 position with motion tracking.
274
275 **Motion tracking experiments**

276   An underwater camera rig was designed to record video footage of the orthocone models
277   as they rose/fell in the water (Fig. 2A). Experiments were performed in a 2.1-meter-deep section
278   of the crimson lagoon – a 50 meter lap pool at the University of Utah. The skeleton of the rig
279   was constructed with two-inch PVC pipe with custom 3D-printed fittings for two camera
280   mounts. Three steel weights were positioned at each end of the T-shaped rig and rubber mats
281   were wrapped around each section to prevent the rig from slipping on the pool liner. Each
282   camera mount consists of a GoPro Hero 8 Black camera in a waterproof case on top of a
283   waterproof LED light (Fig. 2B). Each camera was oriented with the long axis in the vertical
284   direction for improved field of view. Videos were recorded at 60 frames per second with a linear
285   field of view and 4K resolution. Each model was held with extendable tongs until steady, then
286   released for a total of 15 trials for the positively buoyant scenarios, and 8 trials for the negatively
287   buoyant scenario. The relationship between model texture and velocity were assessed by coating
288   the orthocone model with peak *Nautilus*-like thrust (Scenario 3) with hydrophobic silicone spray
289   and performing an additional 15 trials. Sample video footage for Scenario 3 is stored in an online
290   repository (https://doi.org/10.5281/zenodo.4776924).

291   Dual video footage was imported into the 3D motion tracking software DLTdv8
292   (*Hedrick, 2008*) and semi-automatic tracking was used to mark the pixel locations of each
293   tracking point (apex and arms). A calibration was performed in easyWand5 (*Theriault et al.,*
294   *2014*) to transform the 2D pixel coordinates from each video into a single set of 3D coordinates
295   in meters. The model itself was used for wand calibration, ensuring any 3D orientation of the
296   model yielded its actual body length (57 cm). Three-dimensional data points higher in the water
297   column were subject to minor image artifacts from light interacting with the water surface. These
298   distortions, in addition to the increasingly oblique apparent angles of each model, yielded higher
299   error in these regions. Calibrations with standard deviations of less than 2 cm were considered
300   acceptable. The very fast frame rate (60 fps) caused fluctuations in velocity at lower time steps.
301   This was remediated by using a moving average with a window of 11 time steps for the
302   positively buoyant experiments. No moving average was used on the negatively buoyant
303   experiment because only every 10th frame was used to compute velocity (due to very low
304   velocities and long trial times).

305   Velocities were computed as a function of time for each model using the calibrated, 3D
306   datapoints:

307
$$V_i = \frac{\sqrt{(x_i - x_{i-1})^2 + (y_i - y_{i-1})^2 + (z_i - z_{i-1})^2}}{(t_i - t_{i-1})} \tag{5}$$

308   Where V and t are velocity and time, and the subscripts i and i-1 refer to the current and previous
309   time steps, respectively. The 3D theorem of Pythagoras was used to compute the total distance
310   traveled in any x,y,z direction between time steps (which was mostly vertical). The video frame
311   number was divided by the frame rate (59.94 frames per second) to compute time. Time zero for
312   each trial was defined as the moment the release mechanism no longer contacted the model.

313   The curve fitting toolbox in MATLAB R2020a was used fit the velocity data for each
314   model with an asymptotic equation in the form:

315 $$V_{fit} = a - ae^{-bt} \qquad (6)$$

316 Where V_{fit} is the fit velocity and t is time. The term "a" is a coefficient denoting the velocity
317 asymptote (i.e., the maximum velocity estimate given a particular thrust), and b is a coefficient
318 that governs slope.
319   The relationships between hydrostatic stability and hydrodynamic movement were
320 assessed by computing the maximum angle displaced from the vertical static orientation in any
321 particular direction (θ_{dv}):

322 $$\theta_{dv} = \cos^{-1}\left(\frac{(z_2 - z_1)}{\sqrt{(x_2 - x_1)^2 + (y_2 - y_1)^2 + (z_2 - z_1)^2}}\right) \qquad (7)$$

323 Where the subscripts 1 and 2 of the x, y, and z coordinates refer to the arm and apical tracking
324 points, respectively.
325
326 **Predator evasion potential**
327   By knowing how velocity increases from stationary initial conditions (Equation 6), the
328 time it takes to move one body length (t_{bl}) or half a body length ($t_{bl/2}$) can be computed:

329 $$\Delta P = L_{body} = \int_0^{t_{bl}} a - ae^{-bt} \qquad (8)$$

330 When the change in position (ΔP) is equal to the length of the body (L_{body}; 57 cm), t_{bl} can be
331 computed by integrating Equation 6 and determining the upper limit of integration. This limit
332 was computed iteratively in MATLAB by increasing t_{bl} until the integrated equation was equal to
333 L_{body}. For an orthocone to dodge a horizontally moving predator, jetting at the last moment
334 would be ideal for a vertical escape. The minimum distance required (D) to dodge a predator
335 attack at some incident velocity (V_p) was computed by multiplying t_{bl} or $t_{bl/2}$ by the predator's
336 velocity (V_p). Since the critical swimming speeds of extinct animals are difficult to determine,
337 extant marine predators were used as analogues.
338

339 **Results**
340
341 **Model hydrostatics and error**
342   Each of the four orthocone models have the same centers of buoyancy because their
343 external volumes are identical (Table 1). However, the centers of mass for each component of
344 unique density differed in order to maintain a stability index of 0.505 as total mass varied
345 between models (Tables 1 and 2). The mass of the bismuth counterweights slightly differed from
346 their virtual counterparts to compensate for differences in mass between the virtual and physical
347 PLA components. This mass difference reduced error in total mass by sacrificing accuracy in
348 hydrostatic stability (Table 3). The differences in PLA mass were likely a result of differences in
349 bulk density between each of the models. Even with identical slicer settings, the path of the
350 extruder in each layer was slightly different between models, which contributed to error in PLA
351 mass and density. Percent difference of hydrostatic stability and thrust between the virtual and
352 physical models is reported on Table 3.

353

Motion tracking kinematics

354
355   The upward force on the physical models occurs on the center of buoyancy, not the
356 location of the hyponome. However, this location of applied force is a reasonable assumption for
357 these experiments because perfect upward-vertical thrust is still simulated. Furthermore, the
358 actual source of thrust and the centers of buoyancy and mass are very close to being vertically
359 aligned in living orthoconic cephalopods and in the current models. This alignment would allow
360 thrust to be transmitted into primarily upward translation with little energy lost to rocking.
361   After releasing the models underwater, they primarily moved in the vertical directions
362 with velocities proportionate to their simulated thrust values. Each of the trials were slightly
363 skewed in the horizontal directions due to weak currents created by removing the release
364 mechanism (Fig. 3). Additionally, the initial angles of some trials were slightly tilted from
365 vertical, causing a few outlier trajectories (see Fig. 3A).
366   During vertical movement, high hydrostatic stability prevented substantial displacements
367 from vertical orientations (Fig. 4). The tracking points were about two degrees from true vertical
368 in a static setting, and most trials remained under five degrees from vertical. Larger angles of
369 displacement were usually the result of a tilted starting position (see Fig. 4A). The negatively
370 buoyant model underwent larger displacements from vertical only at higher velocities (~-7 cm/s)
371 and consistently tilted dorsum-upwards.
372   The velocities between all trials of each positively buoyant model were remarkably
373 similar (Fig. 5A-C). However, the negatively buoyant model (Fig. 5D) was more sensitive to
374 initial conditions (i.e., the subtle motion caused by holding the tongs before and during release)
375 due to the relatively low force acting in the downwards direction. While Equation 6 yields high
376 R-squared values (>0.97), it underpredicts velocities at the start and end of the experiments, and
377 slightly overpredicts velocities in the middle. This equation, however, provides a simple model
378 to estimate orthocone swimming velocities using only a few terms (Table 4) and avoids
379 overfitting the data. The velocity asymptote for each positively buoyant model is reported in
380 Table 4. With sustained peak *Nautilus*-like thrust, the orthocone model reaches 1.2 m/s (2.1 body
381 length per second) within one second from a stationary initial condition (Fig. 5C; Table 4). A
382 sustained thrust during this narrow time window is a suitable assumption because it is on par
383 with the propulsive period observed in extant *Nautilus* (~0.62-1.39 seconds; *Chamberlain,*
384 *1987*). While Equation 6 reports asymptotic velocities, experiments with longer durations (over
385 larger vertical distances) are required to determine the upper velocity limit (when hydrodynamic
386 drag is equal to thrust). Coating the model with hydrophobic silicone yields little difference in
387 velocity during the time window of the experiments (Fig. 5C). However, the velocity asymptote
388 of Equation 6 between the coating and uncoated models yields a difference in 23 cm/s,
389 suggesting that this asymptote term is very sensitive. The negatively buoyant model is capable of
390 reaching relatively high velocities (~15 cm/s) after about 20 seconds of uninterrupted sinking,
391 falling from <2 meters.
392

393 **Modeling vertical escape maneuvers in orthocones**

394   The time required to move one body length (t_{bl}) or half a body length ($t_{bl/2}$) under each
395 thrust scenario was computed to determine the minimum distance (D) required to dodge a
396 horizontally moving predator (Tables 4 and 5; Fig. 6). With higher thrust values (e.g., peak
397 *Nautilus*-like thrust) these cephalopods could potentially thwart predator attacks from some
398 relatively faster predators. A successful dodge, however, depends on predator maneuverability
399 and burst swimming duration (*Maresh et al., 2004*). If D is much larger than the body length of
400 the predator, it could easily adjust its trajectory in the vertical direction and ultimately catch the
401 relatively slower orthocone.

402

403 ## Discussion

404   The modeled ammonoid species, *Baculites compressus*, provides new context for the
405 swimming capabilities, ecology, and adaptive value of the orthocone morphotype. Maintaining
406 model hydrostatics in a chaotic, real-world setting demonstrates that movement is well
407 constrained despite transient flow conditions surrounding the model (due to model rocking,
408 minor ambient currents, and acceleration from a static initial condition; Figs. 3-5). Aspects of
409 these properties likely varied between orthoconic cephalopods with increasingly different ribbing
410 intensity, curvature, whorl section shape, degree of taper, and size. Furthermore, these
411 cephalopods likely assumed diverse life habits during their ~420 Myr intermittent range, inferred
412 by their disparity and occurrences in variable facies (*Kennedy and Cobban, 1976; Wright,*
413 *Callomon, and Howarth, 1996; Kröger, Servais, and Zhang, 2009*). However, the present
414 experiments reveal first-order constraints for the ubiquitous representatives of this persistent
415 morphotype. Furthermore, a range of model buoyancies (thrusts) simulate possible modes of
416 locomotion that are relevant to a broad range of orthocone taxa. The vertical movement potential
417 revealed by the current experiments is applied further to model different scenarios involving
418 predator evasion.

419

420 **Vertical movement potential**
421 The vertically-streamlined shape of orthoconic cephalopods offers several advantages for
422 movement in the vertical direction. High hydrostatic stability would not have allowed these
423 living cephalopods to considerably deviate from a vertical life habit (*Peterman et al., 2019*)
424 unless they had sufficient counterweights to reduce stability (i.e., cameral and endosiphuncular
425 deposits of some nautiloids; *Peterman, Barton, and Yacobucci, 2019*). Stability acts passively
426 and reduces energy expenditure in all ectocochleates cephalopods, regardless of conch
427 morphology. However, the benefits of high stability in orthocones would come at the cost of
428 maneuverability (*Weihs, 2002; Fish, Hurley, and Costa, 2003; Webb, 2005; Fish and Holzman,*
429 *2019*). When thrust is applied in the upward direction, living orthocones would have maintained
430 a vertical orientation with negligible deviation (<8° resulting from tilted starting positions, but
431 generally <4° in the models; Fig. 4). The minor disturbances caused by removing the release
432 mechanism (Fig. 3) demonstrate that slow translation in the horizontal directions can occur from

433   weak external currents in the water column. This behavior also suggests that horizontal thrust
434   would allow slow horizontal movement, which still could have been functional for the location
435   of a mate or capture of slower prey items. Vertical migration, however, would have been much
436   less expensive due to the vertical streamlining of the conch. Very low input thrust can yield high
437   velocities relative to other ectocochleates of the same mass (Fig. 5; Tables 3 and 4). If certain
438   orthoconic cephalopods underwent similar vertical migration patterns to extant nautilids (*Ward
439   et al., 1984; Ward, 1987; O'Dor et al., 1993; Dunstan, Ward, and Marshall, 2011*), they would
440   require lower thrusts than those experimented upon to leisurely rise and fall in the water column.
441   These diurnal vertical movements allow feeding at relatively shallower depths during the night to
442   avoid predation (*Dunstan, Ward, and Marshall, 2011; Kaartvedt et al., 1996*). This feeding tactic
443   may have been more beneficial for ectocochleates in response to more abundant visual predators
444   after the advent of the Devonian nekton revolution (*Klug et al., 2010*). For baculitids, there is
445   evidence of both demersal behavior and somewhat higher occupation of the water column
446   (*Tsujita and Westermann, 1998; Landman, Cobban, and Larson, 2012; Landman et al., 2018;
447   Rowe et al., 2020)*. Perhaps these ammonoids were able to assume either of these lifestyles,
448   depending on the taxon or available resources. However, it should be noted that isotope values
449   reported for *Baculites* (*Ferguson et al., 2019*) are not comparable to vertical migration ranges
450   recorded in *Nautilus* shell material (*Linzmeier et al., 2016*).
451   A slightly negatively buoyant condition would be easier for the living orthocones to
452   manage (like extant nautilids; *Ward and Martin, 1978*), and represents the more conservative
453   speculation. The downward-facing soft body may have prevented orthocones from efficiently
454   directing a water jet upward, to counteract positive buoyancy, which may be problematic in the
455   event of shell loss due to predation. This scenario may have been managed by ammonoid
456   orthocones, if their complex septa improved buoyancy regulation (i.e., chamber refilling
457   potential; *Daniel et al., 1997; Peterman et al., 2021b*). If complex ammonoid sutures (*Peterman
458   et al., 2021b*) or larger siphuncles in some nautiloids (e.g., actinocerids, endocerids; *Kröger,
459   2003*) improved buoyancy management for these lifestyles, perhaps the magnitude of negative
460   buoyancy could be adjusted for improved downward movement. The low metabolic cost of
461   upward movement from reduced hydrodynamic drag would apply to downward movement as
462   well. A very small surplus in mass (~0.5 g, ~0.26% of organismal mass; *Ward and Martin, 1978*)
463   would allow orthocones to slowly drift downwards. Without jetting, living orthocones would
464   pick up speed (as high as 15 cm/s after 20 seconds for a 57 cm individual, starting <2 m above
465   the seafloor; Fig. 5D). However, if these cephalopods were moving too fast, velocity could be
466   managed by small, periodic jets (i.e., braking). Furthermore, they may have been able to move in
467   the horizontal directions through weak jetting or simply by arranging the positions of the arms.
468   This ability is suggested by the negatively buoyant experiments, which would start tilting toward
469   the dorsum and moving in that direction when the downward velocity reached ~8 cm/s (Figs. 3D,
470   4D, 5D). This behavior is likely due to the shape of the whorl section of *Baculites compressus*,
471   which is wider toward the dorsum and narrower toward the venter (similar to the teardrop-shaped
472   cross-section of an airfoil). This classic shape would have lower pressure differentials with a

473   rounded leading edge compared to other directions (*Maxim, 1896*). Therefore, orthocones with
474   whorl sections similar to *Baculites compressus* may have had a slight drag reduction when
475   moving in the dorsal direction, compared to other lateral directions. Sinking may have provided a
476   low-cost feeding strategy because incident fluid would continuously move toward the mouth
477   (compare *Peterman et al., 2021a*). The reported growth direction of a cirripede attached to the
478   baculitid, *Sciponoceras* (*Hauschke, Schöllmann, and Keupp, 2011*) may have resulted from this
479   direction of movement rather than aperture-forward, horizontal swimming. Similar epizoan
480   growth directions on orthoconic nautiloids (*Baird et al., 1989*) may indicate that these
481   cephalopods frequented this mode of locomotion as well. Slowly sinking toward the benthos may
482   have even qualified as a pounce (especially for early Paleozoic orthocones), catching even
483   slower prey items by surprise (e.g., trilobites, gastropods, other cephalopods, etc.; *Alexander,*
484   *1986; Landman and Davis, 1988; Frey, 1989; Ebbestad and Peel, 1997; Westermann, 1998;*
485   *Brett and Walker, 2002; Kröger, 2004, 2011*).
486
487   **Vertical escape tactics of orthoconic cephalopods**
488   During the ~420 Myr range of orthoconic cephalopods, the predatory landscape changed
489   dramatically. From the Early/Middle Ordovician to the Devonian nekton revolution, large
490   orthocones themselves were the among the dominant predators (*Brett and Walker, 2002; Walker*
491   *and Brett, 2002; Kröger and Zhang, 2009; Kröger, Servais, and Zhang, 2009; Klug et al., 2010*).
492   After this event, larger, faster, and speed-efficient, nektic predators would have imposed new
493   pressure on ectocochleate cephalopods (*Klug et al., 2010, 2017*). These changes are reflected in
494   the evolutionary trend of increased coiling in early ammonoids, and would have continued to
495   influence predator-prey interactions for both persisting nautiloid groups and orthoconic
496   ammonoids at different points in time. The high velocities (among ammonoids) in the
497   experiments (Fig. 5C) suggest that vertical evasion tactics may have been feasible for some
498   orthocones, provided that they have similar propulsive capabilities to modern *Nautilus*.
499   Nautiloids and ammonoids likely were eaten by other cephalopods and crustaceans
500   throughout the Paleozoic and Mesozoic (*Landman and Waage, 1986; Klug, 2007; Kröger,*
501   *Servais, and Zhang, 2009; Hoffmann et al., 2019*). Reports of predation are scarcer for nautiloids
502   compared to ammonoids, especially regarding orthocones (*Mapes and Chaffin, 2003*). However,
503   predator-prey interactions can be inferred from specific predators through time. Other
504   cephalopods and large arthropods would have likely assumed higher predatory roles during the
505   early Paleozoic (*Kröger, 2004, 2011*). After the Devonian nekton revolution began, predation of
506   nautiloids would have intensified from durophagous and piscivorous gnathostome fishes (e.g.,
507   placoderms, sharks, and other jawed fishes; *Seuss et al., 2011*) due to their superior size,
508   maneuverability, and feeding capabilities. After the Devonian mass extinction, sharks,
509   holocephalans, and bony fishes would have served higher-tier predatory roles. Large marine
510   reptiles (e.g., plesiosaurs, ichthyosaurs, mosasaurs, etc.) diversified and were among the
511   dominant components of marine ecosystems during the Mesozoic (*Stubbs and Benton, 2016*).
512   Orthoconic ammonoids, primarily baculitids in the Cretaceous, have well-documented

513   paleopathologies. Damage frequently occurs near the aperture at various growth stages (*Klinger*
514   *and Kennedy, 2001; Kennedy, Cobban, and Klinger, 2002*), likely resulting from pycnodontid
515   fish, coleoids (*Kennedy, Cobban, and Klinger, 2002*), and/or crustaceans (*Keupp, 2012*). Fatal
516   injuries caused by mosasaurs are relatively common for *Baculites* as well (*Kauffman 1990;*
517   *Westermann, 1996; Tsujita and Westermann, 2001*). Quick upward jetting could allow easy
518   escape from a benthic or demersal predator (e.g., crustaceans and some cephalopods). However,
519   thwarting attacks from the relatively quicker nektic predators would require specific escape
520   maneuvers.
521   The likelihood of escape would have increased if a somewhat stationary orthocone waited
522   to jet away from a horizontally moving predator until the last possible moment (Fig. 7A).
523   Otherwise the predator could simply adjust its trajectory and catch up to the slower, vertically
524   moving orthocone (Fig. 7B). Within the time it takes for an orthocone to move some percentage
525   of its body length (100% or 50%), a successful simulated dodge occurs when the distance
526   between a predator (moving at its maximum velocity) and the orthocone is less than the body
527   length of the predator (Fig. 6; Table 5). The condition was chosen because turning radius
528   generally increases with velocity and body length (*Maresh et al., 2004*), thus reducing
529   maneuverability and vertical correction. It should be noted that marine predators have greatly
530   diversified in locomotor capabilities and feeding behavior through time (*Brett and Walker, 2002;*
531   *Stubbs and Benton, 2016; Klug et al., 2017*), so this approach only represents a very general
532   model. Furthermore, repetitive attacks from predators are not considered. Perhaps a single
533   successful dodge would suffice if neighboring prey were captured instead, or within poorly lit
534   waters. While this approach is simple, it suggests that orthoconic cephalopods had a fighting
535   chance of surviving the attacks of some larger predators (using extant marine predators as
536   analogues). Larger marine predators with similar size and speed to some modern cetaceans and
537   saltwater crocodiles may have been outmaneuvered in some cases (Table 5). However, predators
538   with the speed and maneuverability of modern dolphins or some sharks would have been
539   difficult to evade (Table 5). While many aspects of predation behavior are neglected in this
540   model, it should be noted that the vertical orientation of orthocones may have made it difficult
541   for some vertebrate predators to attack because they would have to rotate their heads or entire
542   bodies ~90° to bite down on the flanks of the shell. For small, quick, highly maneuverable
543   predators (e.g., pycnodontid fish), perhaps it was more favorable for an orthoconic cephalopod to
544   hide in its shell rather than attempting to vertically escape. Therefore, vertically escaping from
545   larger predators that mark certain death is likely a last resort for orthoconic cephalopods, which
546   normally assume low-energy lifestyles (*Chamberlain, 1993; Mutvei, 2002; Rowe et al., 2020;*
547   *Hoffmann et al., 2021*).
548
549   **Paleoecological interpretations**
550   The low-cost vertical movement and momentarily rapid escape inferred for orthocones by
551   the current experiments better constrain the ecology of these cephalopods. Existing

552 morphological and ecological information can be used along with these inferred locomotive
553 capabilities to better elucidate the life habits of these ubiquitous animals.
554   The largely unknown soft body characteristics of orthoconic cephalopods could
555 contribute to differences in available thrust and velocities. If the propulsion of ammonoid
556 orthocones is more similar to coleoids (*Jacobs and Landman, 1993*), closer relatives than
557 nautiloids (*Kröger, Vinther, and Fuchs, 2011*), they may have been able to produce larger thrusts
558 than the highest thrust value used in the current experiments (peak *Nautilus*-like thrust).
559 However, it is unknown how confinement of the soft body in a rigid shell would reduce
560 propulsive power compared to coleoids which can hyperinflate their mantle cavities (*Anderson
561 and Demont, 2000*). Furthermore, the lack of well-preserved soft body material (*Klug, Riegraf,
562 and Lehmann, 2012; Klug and Lehmann, 2015;* but see *Klug et al., 2021*) complicates
563 homologization of muscles inferred by scars on the shell (*Kennedy, Cobban, and Klinger, 2002;
564 Doguzhaeva and Mapes, 2015*) to the musculature of extant coleoids or nautiloids. Therefore, the
565 thrust values in the current study pose a wide range of somewhat conservative thrust estimates
566 for ammonoids. For orthoconic nautiloids (orthocerids, endocerids, and actincocerids, among
567 others), muscle scars are different from those of extant *Nautilus* and tarphycerids which suggests
568 that certain orthocone clades may have been weaker swimmers compared to coiled nautiloid
569 clades (*Mutvei, 2002; King and Evans, 2019*). In this case, the *Nautilus*-like peak thrust of the
570 current experiments may be too liberal. However, the magnitude of propulsive differences due to
571 differences in muscle scar size and extent are unclear in the absence of soft part preservation or
572 modern orthocone analogues.
573   Though far from orthocone analogues, extant shrimpfish (a.k.a. razorfish) assume
574 downward-facing vertical orientations. However, in contrast to orthoconic cephalopods, they can
575 pitch their bodies into horizontal orientations during swimming due to their comparatively lower
576 hydrostatic stability (*Fish and Holzman, 2019*). Furthermore, these fish can turn about their
577 longitudinal axis with ease due to their low moments of inertia (*Atz, 1962; Fish and Holzman,
578 2019*). While this behavior was not investigated in the current study, this property seems likely
579 for orthocones as well, based on their mass distribution and general shape. However, rather than
580 using various fins, orthocones would be limited to swimming with their arms and hyponome near
581 the aperture (if the soft body morphology permitted), which is likely not as effective. The
582 transverse cross-section of shrimpfish (*Fish and Holzman, 2019*) is also similar to many baculitid
583 ammonoids (see *Larson et al., 1997*), which infers drag would be reduced in the dorsal direction.
584 Although this horizontal mode of locomotion in orthocones would not be very efficient due to
585 the higher hydrodynamic drag relative to vertical movement, and their low source of jet thrust
586 (i.e., the thrust angle; *Okamoto, 1996; Peterman et al., 2019; Peterman, Mikami, and Inoue,
587 2020*). The vertical orientation of shrimpfish is thought to be associated with camouflage (*Fish
588 and Holzman, 2019*); a function unlikely for comparatively larger orthocones, and those in
589 habitats lacking structure in which to hide.
590   Exceptional preservation has been reported more commonly for baculitid ammonoids
591 than any other orthocone (*Klug, Riegraf, and Lehmann, 2012; Klug and Lehmann, 2015*),

592 allowing more specific interpretations of their life habit. The preservation of large putative eye
593 capsules and the presence of lateral sinuses at their apertures suggest enhanced predator
594 detection capabilities (*Nilsson et al., 2012*). The large ventral rostrum on many baculitid shells
595 may have restricted thrust in the ventral direction, suggesting limited horizontal mobility (unless
596 the hyponome could bend around the rostrum using the lateral sinuses). These features, along
597 with the hydrodynamic properties inferred by the current experiments support a life habit of
598 slowly searching for planktic prey, while maintaining the option for somewhat rapid vertical
599 escape from large predators. For baculitids, this life habit is consistent with well-preserved
600 mouthparts (aptychi and radulae) that support planktivory (*Landman, Larson, and Cobban,*
601 *2007; Kruta et al., 2009; Kruta et al., 2011*). A low energy lifestyle of searching for small,
602 planktic prey can be facilitated by low-cost vertical movement or from relatively sedentary,
603 demersal behavior (e.g., around methane seeps teeming with life; *Landman et al., 2018; Rowe et*
604 *al., 2020*).
605   The vertical motility of orthoconic cephalopods is higher relative to planispiral
606 ammonoids, based on their differences in hydrostatic centers (thrust angle; *Okamoto, 1996;*
607 *Peterman et al., 2019; Peterman, Mikami, and Inoue, 2020*) and vertical streamlining
608 (*Westermann, 1996*). This advantage suggests they could have occupied a distinct niche among
609 ectocochleates. The availability of this niche may reflect suitable ecological opportunities arising
610 from dynamic ecological conditions (e.g., predatory pressure, food resources; *Cecca, 1997;*
611 *Reboulet, Giraud, and Proux, 2005*). Similarly, dynamic environmental conditions (e.g., sea
612 level rise, microhabitat availability; *Yacobucci, 2015*) also drive selection and speciation in
613 ectocochleates, which may have increased the availability of this niche in newly-formed epeiric
614 seas.
615   Our results offer interpretations for the adaptive value of orthoconic cephalopods and
616 potential evolutionary drivers behind their iterative recurrence in the fossil record. Due to the
617 many uncertainties regarding predator evasion and the putative low-energy lifestyle of
618 orthocones (*Chamberlain, 1993; Mutvei, 2002; Rowe et al., 2020; Hoffmann et al., 2021*), we
619 suggest their low-cost vertical motility and unique hydrostatic properties to be a primary driver
620 of their evolution and success. While orthocones may have maintained the ability to dodge
621 benthic or nektic predators, these capabilities are likely restricted to taxa without substantial
622 conch curvature. Instead, transitional forms (e.g., cyrtocones; *Hoffmann et al., 2021*) show
623 gradual changes in hydrostatic properties; static orientations with progressively downward-
624 facing apertures and thrust angles improved for upward locomotion. These trends throughout
625 orthocone ammonoid evolution are generally the inverse of those observed during ammonoid
626 origination (*Klug and Korn, 2004; Kröger and Mapes, 2007; Monnet, De Baets, and Klug, 2011;*
627 *Monnet, Klug, and De Baets, 2015*). Furthermore, these transitional forms would not likely
628 facilitate rapid movement.
629   Orthocones with a higher degree of morphological disparity from our target species,
630 *Baculites compressus*, could have progressively differing hydrostatic and hydrodynamic
631 properties that constrained their life habits and swimming capabilities. Conch size, curvature,

632   whorl section shape, ornamentation, body chamber proportion, and internal characteristics (e.g.,
633   septal/siphuncular morphology and counterweights) vary within this morphotype. The fluted
634   flanks of some orthocones and variable whorl section shapes (e.g., *B. grandis, B. obtrusus, etc.*)
635   could have influenced hydrodynamics in some way. Furthermore, some orthocones are curved
636   (grading into the cyrtocone morphotype), which could pose difficulties in steering rapid, upward
637   maneuvers. In order to understand the roles and consequences of these characteristics, their full
638   spectra would need to be investigated with future experiments. Furthermore, stability-reducing
639   counterweights (*Peterman, Barton, and Yacobucci, 2019*) in the phragmocones of certain taxa
640   must be investigated further in a dynamic setting to determine their potential influences on
641   posture while swimming.
642

Conclusions

644   The high hydrostatic stability of orthoconic cephalopods without cameral deposits
645   (*Peterman et al., 2019; Peterman, Barton, and Yacobucci, 2019*) would have strictly constrained
646   the life habits of these animals. They would have been confined to vertical orientations without
647   the capacity to substantially modify them. These properties raise questions about the modes of
648   life, functional morphology, and adaptive value of the orthocone morphotype. The
649   hydrodynamics inferred by 3D-printed models of the baculitid, *Baculites compressus*, suggest
650   that vertical movement was well constrained for orthocones (Figs. 3 and 5). High hydrostatic
651   stability prevents rocking during movement, even with somewhat variable starting angles (Fig.
652   4). It seems orthocones are adapted to both upward-vertical movement through active
653   locomotion and passive downward-vertical movement at very little cost. High velocities relative
654   to other ectocochleates of similar size suggest that low hydrodynamic drag is incurred by
655   movement in the upwards direction. Therefore, these living cephalopods required very low
656   energy to vertically migrate in the water column (probably at velocities lower than those in the
657   current study; Fig. 5). Slight negative buoyancy (like extant nautilids, *Ward and Martin, 1978*)
658   would have allowed these cephalopods do slowly sink after jet thrust is suspended. This
659   condition would have allowed low-energy movement and feeding for vertical migrants while
660   also providing suitable speeds to pounce on benthic prey from above. While these cephalopods
661   likely assumed low energy lifestyles, *Nautilus*-like peak thrust would have given orthocones a
662   fighting chance at vertically escaping attacks by larger predators. Although coiled ectocochleate
663   cephalopods flourished from the Devonian to end of the Cretaceous, orthoconic cephalopods
664   retained adaptive value during this time as low-energy vertical migrants, with the potential to
665   serve as periodic escape artists.
666

Acknowledgements

668   We appreciate the help of Emma Janusz and Mark Weiss for accommodating our experiments at
669   the University of Utah pool (the Crimson Lagoon). We would also like to thank K. De Baets, B.
670   Kröger, A. Pohle, and R. Lemanis for their thoughtful comments and constructive reviews of the
671   manuscript.

672

References

Alexander RR. 1986. Resistance to and repair of shell breakage induced by durophages in Late Ordovician brachiopods. Journal of Paleontology 60: 273–285.

Anderson EJ, Demont ME. 2000. The mechanics of locomotion in the squid *Loligo pealei*: locomotory function and unsteady hydrodynamics of the jet and intramantle pressure. The Journal of Experimental Biology 203: 2851–2863.

Anderson EJ, Grosenbaugh MA. 2005. Jet flow in steadily swimming adult squid. Journal of Experimental Biology 208: 1124–1146. DOI 10.1242/jeb.01507.

Atz JW. 1962. Does the shrimpfish swim head up or head down? Animal Kingdom 66: 175–179.

Baird GC, Brett CE, Frey RC. 1989. Hitchhiking epizoans on orthoconic cephalopods: preliminary review of the evidence and its implications. Senckenbergiana lethaea 69, 439–465.

Barskov IS, Boiko MS, Konovalova VA, Leonova TB, Nikolaeva SV. 2008. Cephalopods in the marine ecosystems of the Paleozoic. Paleontological Journal 42: 1–1167. DOI 10.1134/S0031030108110014.

Benga G, Chapman BE, Cox GC, Kuchel PW. 2010. Comparative NMR studies of diffusional water permeability of red blood cells from different species: XVIII platypus (*Ornithorhynchus anatinus*) and saltwater crocodile (*Crocodylus porosus*). Cell Biology International 34: 703–708. DOI 10.1042/CBI20090430.

Blender Online Community. 2017. Blender, a 3D modelling and rendering package. Blender Institute, Amsterdam. Available at: http://www.blender.org. Accessed 1 June 2018.

Brett C, Walker S. 2002. Predators and predation in Paleozoic marine environments. Paleontological Society Papers 8: 93–118.

Cecca F. 1997. Late Jurassic and Early Cretaceous uncoiled ammonites: Trophism-related evolutionary processes. Comptes Rendus de l'Académie des Sciences-Series IIA-Earth and Planetary Science, 325: 629–634.

Chamberlain Jr. JA. 1987. Locomotion in *Nautilus*. In: Saunders, W.B., Landman, N.H., eds. *Nautilus*—the biology and paleobiology of a living fossils. Springer, Dordrecht, 489–526.

Chamberlain Jr. JA. 1993. Locomotion in ancient seas: constraint and opportunity in cephalopod adaptive design. Geobios 15: 49–61.

Cignoni P, Ranzuglia G. 2014. MeshLab. Version 1.3.3. Visual Computing Lab, Pisa, Italy. Available from: http://meshlab.sourceforge.net/. Accessed 1 August 2018.

Crick RE. 1988. Buoyancy regulation and macroevolution in nautiloid cephalopods. Senckenbergiana lethaea 69: 13–42.

Daniel TL, Helmuth BS, Saunders WB, Ward PD. 1997. Septal complexity in ammonoid cephalopods increased mechanical risk and limited depth. Paleobiology 23: 470–481.

Doguzhaeva LA. 1994. An Early Cretaceous orthocerid cephalopod from north-western Caucasus. Palaeontology 37: 889–899.

711 Doguzhaeva L, Mapes RH. 2015. The body chamber length variations and muscle and mantle
712   attachments in ammonoids In: Klug C, Korn D, De Baets K, Kruta I, Mapes RH, eds.
713   Ammonoid Paleobiology: from anatomy to ecology. Topics in Geobiology 43, Springer,
714   Dordrecht. 545–584. DOI 10.1007/978-94-017-9630-9_14.
715 Dunstan AJ, Ward PD, and Marshall NJ. 2011. Vertical distribution and migration patterns of
716   *Nautilus pompilius*. PLoS ONE 6: e16311. DOI 10.1371/journal.pone.0016311.
717 Ebbestad JOR, Peel JS. 1997. Attempted predation and shell repair in Middle and Upper
718   Ordovician gastropods from Sweden. Journal of Paleontology 71: 1047–1060.
719 Erben HK. 1996. Über den Ürsprung der Ammonoidea. Biological Reviews 41: 641–658. DOI
720   10.1111/j.1469-185X.1966.tb01626.x.
721 Fatherree JW, Harries PJ, Quinn TM. 1998. Oxygen and carbon isotopic "dissection" of
722   *Baculites compressus* (Mollusca: Cephalopoda) from Pierre Shale (Upper Campanian) of
723   South Dakota: implications for paleoenvironmental reconstructions. Palaios 13: 376–385.
724 Ferguson K, MacLeod KG, Landman NH, Sessa JA. 2019. Evaluating growth and ecology in
725   baculitid and scaphitid ammonites using stable isotope sclerochronology. Palaios 34: 317–
726   329. DOI 10.2110/palo.2019.005.
727 Fernandez-Waid P, Diez G, Bidaguren I, Izagirre U, Blanco JM, Soto M. 2019. Morphological
728   characterization of hydrodynamic behavior of shortfin mako shark (*Isurus oxyrinchus*) dorsal
729   fin denticles. Journal of Bionic Engineering 16: 730–741. DOI 10.1007/s42235-019-0059-7.
730 Fischer AG, Teichert C. 1969. Cameral deposits in cephalopod shells. The University of Kansas
731   Paleontological Contributions 37: 1–37.
732 Fish FE, Holzman R. 2019. Swimming turned on its head: stability and maneuverability of the
733   shrimpfish (*Aeoliscus punctulatus*). Integrative Organismal Biology 1: 1–14. DOI
734   10.1093/iob/obz025.
735 Fish FE, Hurley J, Costa DP. 2003. Maneuverability by the sea lion, *Zalophus californianus*:
736   turning performance of an unstable body design. Journal of Experimental Biology 206: 667–
737   674.
738 Flower RH. 1955a. Cameral deposits in orthoconic nautiloids. Geological Magazine 92: 89–103.
739 Flower RH. 1955b. Saltations in nautiloid coiling. Evolution 9: 244–260.
740 Flower RH. 1955c. Trails and tentacular impressions of orthoconic cephalopods. Journal of
741   Paleontology 29: 857–867.
742 Frey RC. 1989. Paleoecology of well-preserved nautiloid assemblages from a Late Ordovician
743   shale unit, south-west Ohio. Journal of Paleontology 63: 604–620.
744 Hauschke N, Schöllmann L, Keupp H. 2011. Oriented attachment of a stalked cirripede on an
745   orthoconic heteromorph ammonite—implications for the swimming position of the latter.
746   Neues Jahrbuch für Geologie und Paläontologie Abhandlungen 202: 199–212. DOI
747   10.1127/0077-7749/2011/0192.
748 Hedrick TL. 2008. Software techniques for two- and three- dimensional kinematic measurements
749   of biological and biomimetic systems. Bioinspiration and biomimetics 3: 034001. DOI
750   10.1088/1748-3182/3/3/034001.

751 Henderson RA, Price GD. 2012. Paleoenvironment and paleoecology inferred from oxygen and
752   carbon isotopes of subtropical mollusks from the late Cretaceous (Cenomanian) of Bathurst
753   Island, Australia. Palaios 27: 617–626. DOI 10.2110/palo.2011.p11-120r.
754 Hoffmann R, Lemanis R, Naglik C, Klug C. 2015. Ammonoid buoyancy. In: Klug C, Korn D,
755   De Baets K, Kruta I, Mapes RH, eds. Ammonoid Paleobiology: from anatomy to ecology.
756   Topics in Geobiology 44, Springer, Dordrecht. 613–648. DOI 10.1007/978-94-017-9630-
757   9_16.
758 Hoffmann R, Stevens K, Keupp H, Simonsen S, Schweigert G. 2019. Regurgitalites – a window
759   into the trophic ecology of fossil cephalopods. Journal of the Geological Society 177: 82–
760   102. DOI 10.1144/jgs2019-177.
761 Hoffmann R, Slattery JS, Kruta I, Linzmeier BJ, Lemanis RE, Mironenko A, Goolaerts S, De
762   Baets K, Peterman DJ, Klug C. 2021. Recent advances in heteromorph ammonoid
763   paleobiology. Biological Reviews 96: 576–610. DOI 10.1111/brv.12669.
764 Holland CH. 1987. The nautiloid cephalopods: a strange success. Journal of the Geological
765   Society 144: 1–15. DOI 10.1144/gsjgs.144.1.0001.
766 Kaartvedt S, Melle W, Knutsen T, Skjoldal HR. 1996. Vertical distribution of fish and krill
767   beneath water of varying optical properties. Marine Ecology Progress Series 136: 51–58.
768 Kauffman EG. 1990. Mosasaur predation on ammonites during the Cretaceous-an evolutionary
769   history. In: Boucot AJ, ed., Evolutionary paleobiology of behavior and coevolution. Elsevier,
770   New York. 184–189.
771 Kennedy WJ, Cobban WA. 1976. Aspects of ammonite biology, biogeography, and
772   biostratigraphy. Special Papers in Palaeontology No. 17: 94p.
773 Kennedy WJ, Cobban WA, Klinger HC. 2002. Muscle attachment and mantle-related features in
774   Upper Cretaceous *Baculites* from the United States Western Interior. Abhandlungen der
775   Geologischen Bundesantstalt Wien 57: 89–112.
776 Keupp H. 2012. Atlas zur Paläopathologie der Cephalopoden. Berliner paläobiologische
777   Abhandlungen 12: 1–392.
778 King AH, Evans DH. 2019. High-level classification of the nautiloid cephalopods: a proposal for
779   the revision of the Treatise Part K. Swiss Journal of Palaeontology 138: 65–85. DOI
780   10.1007/s13358-019-00186-4.
781 Klinger HC, Kennedy WJ. 2001. Stratigraphic and geographic distribution, phylogenetic trends
782   and general comments on the ammonite family Baculitidae Gill, 1871 (with an annotated list
783   of species referred to the family). Annals of the South African Museum 107: 1–29.
784 Klug C. 2007. Sublethal injuries in early Devonian cephalopod shells from Morocco. Ata
785   Palaeontologica Polonica 52: 749–759.
786 Klug C, Korn D. 2004. The origin of ammonoid locomotion. Acta Palaeontologica Polonica 49:
787   235–242.
788 Klug C, Lehmann J. 2015. Soft part anatomy of ammonoids: reconstructing the animal based on
789   exceptionally preserved specimens and actualistic comparisons. In: Klug C, Korn D, De
790   Baets K, Kruta I, Mapes RH, eds., Ammonoid paleobiology: from anatomy to ecology:

791   Topics in Geobiology 44, Springer, Dordrecht. 515–538. DOI 10.1007/978-94-017-9630-
792   9_12.
793 Klug C, Riegraf W, Lehmann J. 2012. Soft-part preservation in heteromorph ammonites from the
794   Cenomanian-Turonian Boundary Even (OAE 2) in the Teutoburger Wald (Germany).
795   Palaeontology 55: 1307–1331. DOI 10.1111/j.1475-4983.2012.01196.x.
796 Klug C, Kröger B, Kiessling W, Mullins GL, Servais T, Frýda J, Korn D, Turner S. 2010. The
797   Devonian nekton revolution. Lethaia 43: 465–477. 10.1111/j.1502-3931.2009.00206.x.
798 Klug C, Frey L, Pohle A, De Baets K, Korn D. 2017. Palaeozoic evolution of animal mouthparts.
799   Bulletin of Geosciences 92: 439–442. DOI 10.3140/bull.geosci.1648.
800 Klug C, Schweigert G, Tischlinger H, Pochmann H. 2021. Fail prey or peculiar necrolysis?
801   Isolated ammonite soft body from the Late Jurassic of Eichstätt (Germany) with complete
802   digestive tract and male reproductive organs. Swiss Journal of Palaeontology 140: 1–14. DOI
803   10.1186/s13358-020-00215-7.
804 Kröger B. 2003. The size of the siphuncle in cephalopod evolution. Senckenbergiana lethaea 83:
805   39–52. DOI 10.1007/BF03043304.
806 Kröger B. 2004. Large shell injuries in Middle Ordovician Orthocerida (Nautiloidea,
807   Cephalopoda). GFF 126: 311–316.
808 Kröger B. 2005. Adaptive evolution in Paleozoic coiled cephalopods. Paleobiology 31: 253–268.
809 Kröger B. 2011. Size matters – analysis of shell repair scars in endocerid cephalopods. Fossil
810   Record 14: 109–118.
811 Kröger B, Mapes RH. 2007. On the origin of bactritoids (Cephalopoda). Paläontologische
812   Zeitschrift 81: 316–327.
813 Kröger B, Zhang Y. 2009. Pulsed cephalopod diversification during the Ordovician.
814   Palaeogeography, Palaeoclimatology, Palaeoecology 273: 174–183. DOI
815   10.1016/j.palaeo.2008.12.015.
816 Kröger B, Servais T, Zhang Y. 2009. The origin and initial rise of pelagic cephalopods in the
817   Ordovician. PLoS ONE 4: e7262. doi:10.1371/journal.pone.0007262.
818 Kröger B, Vinther J, Fuchs D. 2011. Cephalopod origin and evolution: a congruent picture
819   emerging from fossils, development and molecules. Bioessays 33: 602–613. DOI
820   10.1002/bies.201100001.
821 Kruta I, Rouget I, Landman NH, Tanabe K, Cecca F. 2009. Aptychus microstructure in Late
822   Cretaceous Ancyloceratina (Ammonoidea). Lethaia 42: 312–321. DOI 10.1111/j.1502-
823   3931.2009.00154.x.
824 Kruta I, Landman N, Rouget I, Cecca F, Tafforeau P. 2011. The role of ammonites in the
825   Mesozoic marine food web revealed by jaw preservation. Science 331: 70–72. DOI
826   10.1126/science.1198793.
827 Landman NH. 1982. Embryonic shells of *Baculites*. Journal of Paleontology 56: 1235–1241.
828 Landman NH, Waage KM. 1986. Shell abnormalities in scaphitid ammonites. Lethaia 19: 211–
829   224.

830 Landman NH, Davis RA. 1988. Jaw and crop in an orthoconic nautiloid from the Bear Gulch
831   Limestone (Mississippian, Montana). Memoir – New Mexico Bureau of Mines and Mineral
832   Resources 44: 103–107.
833 Landman NH, Larson NL, Cobban WA. 2007. Jaws and radula of *Baculites* from the Upper
834   cretaceous (Campanian) of North America. In: Landman NH, Davis RA, Mapes RH, eds.,
835   Cephalopods present and past: new insights and fresh perspectives. Springer, Dordrecht.
836   257–298.
837 Landman NH, Cobban WA, Larson NL. 2012. Mode of life and habitat of scaphitid ammonites.
838   Geobios 45: 87–98. DOI 10.1016/j.geobios.2011.11.006.
839 Landman NH, Cochran JK, Sovacek M, Larson NL, Garb MP, Brezina J, Witts JD. 2018.
840   Isotope sclerochronology of ammonites (*Baculites compressus*) from methane seep and non-
841   seep sites in the Late Cretaceous Western Interior Seaway, USA: Implications for ammonite
842   habitat and mode of life. American Journal of Science 318: 603–639. DOI
843   10.2475/06.2018.01.
844 Lindgren J, Caldwell MW, Konishi T, Chiappe LM. 2010. Convergent evolution in aquatic
845   tetrapods: insights from an exceptional fossil mosasaur. PLoS ONE 5:e11998. DOI
846   10.1371/journal.pone.0011998.
847 Linzmeier BJ, Kozdon R, Peters SE, Valley JW. 2016. Oxygen isotope variability within
848   *Nautilus* shell growth bands. PLoS ONE 11: e0153890. DOI 10.1371/journal.pone.0153890.
849 Lukeneder A. 2015. Ammonoid habitats and life history. In: Klug C, Korn D, De Baets K, Kruta
850   I, Mapes RH, eds. Ammonoid Paleobiology: from macroevolution to paleogeography. Topics
851   in Geobiology 44, Springer, Dordrecht. 689–791. DOI 10.1007/978-94-017-9630-9_18.
852 Lukeneder A, Harzhauser M, Müllegger S, Piller WE. 2010. Ontogeny and habitat change in
853   Mesozoic cephalopods revealed by stable isotopes (δ^{18}O, δ^{13}C). Earth and Planetary Science
854   296: 103–114. DOI 10.1016/j.epsl.2010.04.053.
855 Manda S, Turek V. 2015. Colour patterns on Silurian orthocerid and pseudorthocerid conchs
856   from Gotland – palaeoecological implications. Estonian Journal of Earth Sciences 64: 74–79.
857   DOI 10.3176/earth.2015.13.
858 Mapes RH, Chaffin DT. 2003. Predation on Cephalopods. In: Kelley P.H., Kowalewski M.,
859   Hansen T.A. (eds) Predator—Prey Interactions in the Fossil Record. Topics in Geobiology,
860   vol 20. Springer, Boston, DOI 10.1007/978-1-4615-0161-9_8.
861 Maresh JL, Fish FE, Nowacek DP, Nowacek SM. 2004. High performance turning capabilities
862   during foraging by bottlenose dolphins (Tursiops truncatus). Marine Mammal Science 20:
863   498–509.
864 Maxim, HS. 1896. Natural and artificial flight. The Aeronautical Annual (Boston).
865 Monnet C, De Baets K, Klug C. 2011. Parallel evolution controlled by adaptation and
866   covariation in ammonoid cephalopods. BMC Evolutionary Biology 11: 1–21. DOI
867   10.1186/1471-2148-11-115.
868 Monnet C, Klug C, De Baets K. 2015. Evolutionary patterns of ammonoids: phenotypic trends,
869   convergence, and parallel evolution. In: Klug C, Korn D, De Baets K, Kruta I, Mapes RH,

870   eds. Ammonoid Paleobiology: from macroevolution to paleogeography. Topics in
871   Geobiology 44, Springer, Dordrecht. 95–142. DOI 10.1007/978-94-017-9633-0_5.
872 Motani R. 2002. Swimming speed estimation of extinct marine reptiles: energetic approach
873   revisited. Paleobiology 28: 251–262.
874 Mutvei H. 2002. Connecting ring structure and its significance for classification of the orthocerid
875   cephalopods. Acta Palaeontologica Polonica 47: 157–168.
876 Mutvei H. 2018. Cameral deposits in Paleozoic cephalopods. GFF 140: 254–263. DOI
877   10.1080/11035897.2018.1483966.
878 Neil TR, Askew GN. 2018. Swimming mechanics and propulsive efficiency in the chambered
879   nautilus. Royal Society Open Science 5: 170467. DOI 10.1098/rsoc.170467.
880 Nilsson DE, Warrant EJ, Johnsen S, Hanlon R, Shashar N. 2012. A unique advantage for giant
881   eyes in giant squid. Current Biology 22: 683–688. DOI 10.1016/j.cub.2012.02.031.
882 O'Dor RK, Forsythe J, Webber DM, Wells J, Wells MJ. 1993. Activity levels of *Nautilus* in the
883   wild. Nature 362: 626–628.
884 Okamoto, T. 1996. Theoretical modeling of ammonoid morphology. In: Landman NH, Tanabe
885   K, and Davis RA (eds.), Ammonoid Paleobiology. Topics in Geobiology 13. Plenum, New
886   York. p. 225–251.
887 Packard A. 1988. Visual tactics and evolutionary strategies. In: Wiedmann J, Kullmann J, eds.,
888   Cephalopods – Present and Past. Schweizerbart'sche, Stuttgart. 89–103.
889 Peterman DJ, Ciampaglio C, Shell RC, Yacobucci MM. 2019. Mode of life and hydrostatic
890   stability of orthoconic ectocochleate cephalopods: hydrodynamic analyses of restoring
891   moments from 3D-printed, neutrally buoyant models of a baculite. Acta Palaeontologica
892   Polonica 64: 441–460. DOI 10.4202/app.00595.2019.
893 Peterman DJ, Barton CC, Yacobucci MM. 2019. The hydrostatics of Paleozoic ectocochleate
894   cephalopods (Nautiloidea and Endoceratoidea) with implications for modes of life and early
895   colonization of the pelagic zone. Palaeontologia Electronica 22.2.27A: 1–29. DOI
896   10.26879/884.
897 Peterman DJ, Mikami T, Inoue S. 2020. The balancing act of *Nipponites mirabilis*
898   (Nostoceratidae, Ammonoidea): managing hydrostatics throughout a complex ontogeny.
899   PLoS ONE 15: e0235180. DOI 10.1371/journal.pone.0235180.
900 Peterman DJ, Hebdon N., Ciampaglio CN, Yacobucci MM, Landman NH, Linn T. 2020a. Syn
901   vivo hydrostatic and hydrodynamic properties of scaphitid ammonoids from the U.S.
902   Western Interior. Geobios 60: 79–98. DOI 10.1016/j.geobios.2020.04.004.
903 Peterman DJ, Shell RC, Ciampaglio CN, Yacobucci MM. 2020b. Sable hooks: biomechanics of
904   heteromorph ammonoids with U-shaped body chambers. Journal of Molluscan Studies 86:
905   267–279. DOI 10.1093/mollus/eyaa018.
906 Peterman DJ, Hebdon N, Shell RC, Ritterbush A. 2021a. Twirling torticones: hydrostatics and
907   hydrodynamics of helically-coiled ammonoids. In: Slattery JS, Larson NL, Bingle-Davis M.,
908   Graham, FC. eds. Insights into the Cretaceous: Building on the Legacy of William A.

909   Cobban (1916-2015), American Association of Petroleum Geologists and Wyoming
910   Geological Association Special Volume, forthcoming.
911 Peterman DJ, Ritterbush KA, Ciampaglio CN, Johnson EH, Inoue S, Mikami T, Linn TJ. 2021b.
912   Complex shell architecture refined buoyancy control in ammonoid cephalopods. Scientific
913   Reports 11: 8055. DOI 10.1038/s41598-021-87379-5.
914 Pohle A, Klug C. 2018. Early and Middle Devonian cephalopods from Hamar Laghdad (Tafialt,
915   Morocco) and remarks on epicoles and cameral deposits. Neues Jahrbuch für Geologie und
916   Paläontologie Abhandlungen 290: 203–240. DOI 10.1127/njgpa/2018/0776.
917 Reboulet S, Giraud F, Proux O. 2005. Ammonoid abundance variations related to changes in
918   trophic conditions across the Oceanic Anoxic Event 1d (Latest Albian, SE France). Palaios
919   20: 121–141.
920 Rowe AJ, Landman NH, Cochran JK, Witts JD, Garb MP. 2020. Late Cretaceous methane seeps
921   as habitats for newly hatched ammonites. Palaios 35: 151–163. DOI 10.2110/palo.2019.105.
922 Schmidt H. 1930. Über die Bewegungsweise der Schalencephalopoden. Paläontologische
923   Zeitschrift 12: 194–208 [in German].
924 Segre PS, Potvin J, Cade DE, Calambokidis J, Clemente JD, Fish FE, Fridlaender AS, Gough
925   WT, Kahane-Rapport SR, Oliveira C, Parks SE, Penry GS, Simon M, Stimpert AK, Wiley
926   DN, Bierlich KC, Madsen PT, Goldbogen JA. 2020. Energetic and physical limitations on
927   the breaching performance of large whales. eLife 9: e51760. DOI 10.7554/eLife.51760.
928 Sessa JA, Larina E, Knoll K, Garb M, Cochran JK, Huber BT, MacLeod KG, Landman NH.
929   2015. Ammonite habitat revealed via isotopic composition and comparisons with co-
930   occurring benthic and planktonic organisms. PNAS 112: 15562–15567. DOI
931   10.1073/pnas.1507554112.
932 Seuss B, Mapes RH, Klug C, Nützel A. 2011. Exceptional cameral deposits in a sublethally
933   injured Carboniferous orthoconic nautiloid from the Buckhorn Asphalt Lagerstätte in
934   Oklahoma, USA. Acta Palaeontologica Polonica, 57: 375–390. DOI 10.4202/app.2011.0008.
935 Stubbs TL, Benton MJ. 2016. Ecomorphological diversifications of Mesozoic marine reptiles:
936   the roles of ecological opportunity and extinction. Paleobiology 42: 547–573. DOI
937   10.1017/pab.2016.15.
938 Tanaka H, Li G, Uchida Y, Nakamura M, Ikeda T, Liu H. 2019. Measurement of time-varying
939   kinematics of a dolphin in burst accelerating swimming. PLoS ONE 14: e0210860. DOI
940   10.1371/journal.pone.0210860.
941 Teichert C. 1933. Der Bau der actinoceroiden Cephalopoden. Palaeontographica A 78, 111–230
942   [in German].
943 Teichert C, Kummel B, Sweet WC, Stenzel HB, Furnish WM, Glenister BF, Erben HK, Moore
944   RC, Zeller DE. 1964. Part K, Mollusca 3, Cephalopoda – General Features, Endoceratoidea,
945   Actinoceratoidea, Nautiloidea, Bactritoidea. In: Moore, R.C., ed. Treatise on Invertebrate
946   Paleontology. Geological Society of America and The University of Kansas Press, Boulder.
947   519p.

948 Theriault DH, Fuller NW, Jackson BE, Bluhm E, Evangelista D, Wu Z, Betke M, Hedrick TL.
949   2014. A protocol and calibration method for accurate multi-camera field videography. The
950   Journal of Experimental Biology 217: 1843–1848. DOI 10.1242/jeb.100529.
951 Trueman AE. 1941. The ammonite body chamber, with special reference to the buoyancy and
952   mode of life of the living ammonite. Quarterly Journal of the Geological Society 384: 339–
953   383.
954 Tsujita CJ, Westermann GEG. 1998. Ammonoid habitats and habits in the Western Interior
955   Seaway: a case study from the Upper Cretaceous Bearpaw Formation of southern Alberta,
956   Canada. Palaeogeography, Palaeoclimatology, Palaeoecology 144: 135–160.
957 Tsujita CJ, Westermann GEG. 2001. Were limpets or mosasaurs responsible for perforations in
958   the ammonite *Placenticeras*? Palaeogeography, Palaeoclimatology, Palaeoecology 169: 245–
959   270.
960 Walker SE, Brett CE. 2002. Post-Paleozoic patterns in marine predation: was there a Mesozoic
961   and Cenozoic marine predatory revolution? Paleontological Society Papers 8: 119–194.
962 Ward PD, Martin A. 1978. On the buoyancy of the Pearly *Nautilus*. Journal of Experimental
963   Zoology 205: 5–12. DOI 10.1002/jez.1402050103
964 Ward PD. 1987. The natural history of *Nautilus*. Allen and Unwin, Winchester. 267 p.
965 Ward PD, Carlson B, Weekly M, Brumbaugh B. 1984. Remote telemetry of daily vertical and
966   horizontal movement of *Nautilus* in Palau. Nature 309: 248–250.
967 Webb PW. 2005. Stability and maneuverability. In: Shadwick RE, Lauder GV (eds.), Fish
968   Physiology, Fish Biomechanics Vol. 23, Academic Press, p. 281–332.
969 Webber DM, O'Dor RK. 1986. Monitoring the metabolic rate and activity of free-swimming
970   squid with telemetered jet pressure. Journal of Experimental Biology 126: 205–224.
971 Weihs D. 2002. Stability versus maneuverability in aquatic locomotion. Integrative and
972   Comparative Biology 42: 127–134. DOI 10.1093/icb/42.1.127.
973 Wells MJ, O'Dor RK. 1991. Jet propulsion and the evolution of the cephalopods. Bulletin of
974   Marine Science 49: 419–432.
975 Westermann GEG. 1977. Form and function of orthocone cephalopod shells with concave septa.
976   Paleobiology 3: 300–321.
977 Westermann GEG. 1996. Ammonoid life and habitat. In: Landman NH, Tabane K, Davis RA,
978   eds., Ammonoid Paleobiology. Plenum, New York. 607–707.
979 Westermann GEG. 1998. Life habits of nautiloids. In: Savazzi, ed., Functional Morphology of
980   the Invertebrate Skeleton. John Wiley & Sons, Chichester, New York. 263–298.
981 Wiedmann J. 1969. The heteromorphs and ammonoid extinction. Biological Reviews 44: 463–
982   602.
983 Wright CW, Callomon JH, Howarth MK. 1996. Part L Mollusca 4 Revised, Vol. 4: Cretaceous
984   Ammonoidea. In: Moore, R.C., ed. Treatise on Invertebrate Paleontology. Geological Society
985   of America and The University of Kansas Press, Boulder. 362 p.
986 Yacobucci MM. 2015. Macroevolution and Paleobiogeography of Jurassic-Cretaceous
987   Ammonoids. In: Klug C, Korn D, De Baets K, Kruta I, Mapes RH, eds. Ammonoid

988   Paleobiology: from macroevolution to paleogeography. Topics in Geobiology 44, Springer,
989   Dordrecht. 189–228.
990
991

Figure and Table Captions

993

994   **Figure 1:** Construction of a physical, 3D-printed model of *Baculites compressus* from a virtual
995   hydrostatic model. A) Virtual model used to determine hydrostatic properties (modified from
996   *Peterman et al., 2019*). B) Virtual model with simplified internal geometry that allows for 3D
997   printing. The total model mass was manipulated to impart an upward buoyant force, simulating
998   downward thrust. The total center of mass (m) relative to the center of buoyancy (b) was
999   maintained with an adorally placed counterweight and various internal voids. C) Physical, 3D-
1000   printed model with tracking points placed at the distal ends of the arms and apex used for 3D
1001   motion tracking.
1002

1003   **Figure 2:** Underwater camera rig used for 3D motion tracking. A) Schematic of the camera rig
1004   relative to the model (yellow) and release mechanism (green). The rig was made strongly
1005   negatively buoyant with three steel counterweights at the ends (purple). The wireframe shapes
1006   radiating from the cameras denote the approximate field of view. B) Close-up view of
1007   waterproof camera and LED light with custom, 3D-printed attachments.
1008

1009   **Figure 3:** Three-dimensional positions from a common starting point for each model through
1010   time. A) Scenario 1: *Nautilus*-like cruising thrust. B) Scenario 2: *Nautilus*-like cruising thrust
1011   scaled by the higher mantle cavity ratio of *Sepia*. C) Scenario 3: *Nautilus*-like peak thrust. D)
1012   Scenario 4: slightly negatively buoyant (~0.26% of mass not relieved by buoyancy).
1013

1014   **Figure 4:** Maximum displacement angle in any direction from the vertical axis through time.
1015   Each trial is distinguished by color. A) Scenario 1: *Nautilus*-like cruising thrust. B) Scenario 2:
1016   *Nautilus*-like cruising thrust scaled by the higher mantle cavity ratio of *Sepia*. C) Scenario 3:
1017   *Nautilus*-like peak thrust. D) Scenario 4: slightly negatively buoyant (~0.26% of mass not
1018   relieved by buoyancy).
1019

1020   **Figure 5:** Velocity in the direction of movement as a function of time. All trials are fit with an
1021   asymptote equation. A) Scenario 1: *Nautilus*-like cruising thrust. B) Scenario 2: *Nautilus*-like
1022   cruising thrust scaled by the higher mantle cavity ratio of *Sepia*. C) Scenario 3: *Nautilus*-like
1023   peak thrust. A hydrophobic coating was applied to the original model to compare the influence of
1024   surface texture and friction drag. D) Scenario 4: slightly negatively buoyant (~0.26% of mass not
1025   relieved by buoyancy).
1026

1027   **Figure 6:** Diagram of vertical predator escape and related terms. The time required to move one
1028   body length (t_{bl}) or half a body length ($t_{bl/2}$) was computed for each velocity profile (V; Fig. 5).
1029   This time was multiplied by the velocity of various predators (V_p) to compute the minimum
1030   distance required to start jetting (D). A dodge was considered successful if D is less than the
1031   length of the predator (L_p). The image of the mosasaur (*Platecarpus*) was created from the
1032   outline inferred by *Lindgren et al. (2010).*

1033

1034   **Figure 7:** Scenarios involving successful dodging (A) and unsuccessful dodging (B). The
1035   cruising predator first notices the prey (i), then begins to accelerate (ii). After closing in (iii), the
1036   predator makes its final lunge for the prey (iv). Cones surrounding the predator indicate
1037   hypothetical turning radiuses. For a successful dodge, the orthocone cephalopod must wait until
1038   the last possible moment or else the incoming predator could adjust its vertical trajectory. The
1039   image of the mosasaur (*Platecarpus*) was created from the outline inferred by *Lindgren et al.*
1040   *(2010).*

1041

1042   **Table 1:** Local centers of mass for the model components (PLA plastic and bismuth
1043   counterweight), and total centers of mass and buoyancy for each model (1: *Nautilus*-like cruising
1044   thrust; 2: *Nautilus*-like cruising thrust scaled by the higher mantle cavity ratio of *Sepia*; 3:
1045   *Nautilus*-like peak thrust; 4: Slightly negatively buoyant). Only the x and z values are reported
1046   because the virtual model is perfectly symmetrical. All coordinates are measured relative to the
1047   same arbitrary datum (located in the center of the aperture).
1048   .
1049   **Table 2:** Masses (m) and volumes (V) for the virtual and physical model components. 1:
1050   *Nautilus*-like cruising thrust; 2: *Nautilus*-like cruising thrust scaled by the higher mantle cavity
1051   ratio of *Sepia*; 3: *Nautilus*-like peak thrust; 4: Slightly negatively buoyant. PLA = 3D printed
1052   plastic; Bi = bismuth counterweight; wd = water displaced; Mass def. = mass deficiency required
1053   to impart the computed buoyant forces (Table 3); glue = the cyanoacrylate glue used to secure
1054   each counterweight. The residual mass in the negatively buoyant experiment (denoted with *)
1055   was not weighed, but rather its volume was inserted into the model with a syringe (~0.5 cm^3).

1056

1057   **Table 3:** Virtual and actual hydrostatic stabilities (S_t) and thrusts (F), and computed percent
1058   errors. 1: *Nautilus*-like cruising thrust; 2: *Nautilus*-like cruising thrust scaled by the higher
1059   mantle cavity ratio of *Sepia*; 3: *Nautilus*-like peak thrust; 4: Slightly negatively buoyant.

1060

1061   **Table 4:** Velocities, travel times, and asymptote equation coefficients. Uncertainty reflects
1062   bounds of 95% confidence intervals. The asymptotic velocity (in cm/s) is predicted by
1063   coefficient "a" of Equation 6. Coefficient "b" governs the slope. The maximum body lengths per
1064   second (Max. bl/s) were computed by dividing velocity by the body length of the models (57
1065   cm). The time required to move one body length (t_{bl}) and half of one body length ($t_{bl/2}$) was
1066   computed for each model (1: *Nautilus*-like cruising thrust; 2: *Nautilus*-like cruising thrust scaled

1067   by the higher mantle cavity ratio of *Sepia*; 3: *Nautilus*-like peak thrust, coated and uncoated with
1068   hydrophobic silicone spray).

1069

1070   **Table 5:** Predator evasion potential of orthocone cephalopods using mostly extant predators as
1071   analogues. Dodges are considered successful (bold numbers) when the minimum distance
1072   required to start jetting (D) is less than the body length of a predator (L_p) moving at some
1073   incident velocity (V_p). The subscripts in D values refer to different thrust scenarios in the models
1074   (1: *Nautilus*-like cruising thrust; 2: *Nautilus*-like cruising thrust scaled by the higher mantle
1075   cavity ratio of *Sepia*; 3uc: *Nautilus*-like peak thrust with no coating; 3c: *Nautilus*-like peak
1076   thrust, coated in hydrophobic silicone spray). The velocity of *Platecarpus* (denoted by *) is only
1077   an estimate of metabolically optimal velocity (*Motani, 2002*), therefore critical/lunge velocity
1078   should be much higher.

Figure 1

Construction of a physical, 3D-printed model of *Baculites compressus* from a virtual hydrostatic model.

A) Virtual model used to determine hydrostatic properties (modified from *Peterman et al., 2019*). B) Virtual model with simplified internal geometry that allows for 3D printing. The total model mass was manipulated to impart an upward buoyant force, simulating downward thrust. The total center of mass (m) relative to the center of buoyancy (b) was maintained with an adorally placed counterweight and various internal voids. C) Physical, 3D-printed model with tracking points placed at the distal ends of the arms and apex used for 3D motion tracking.
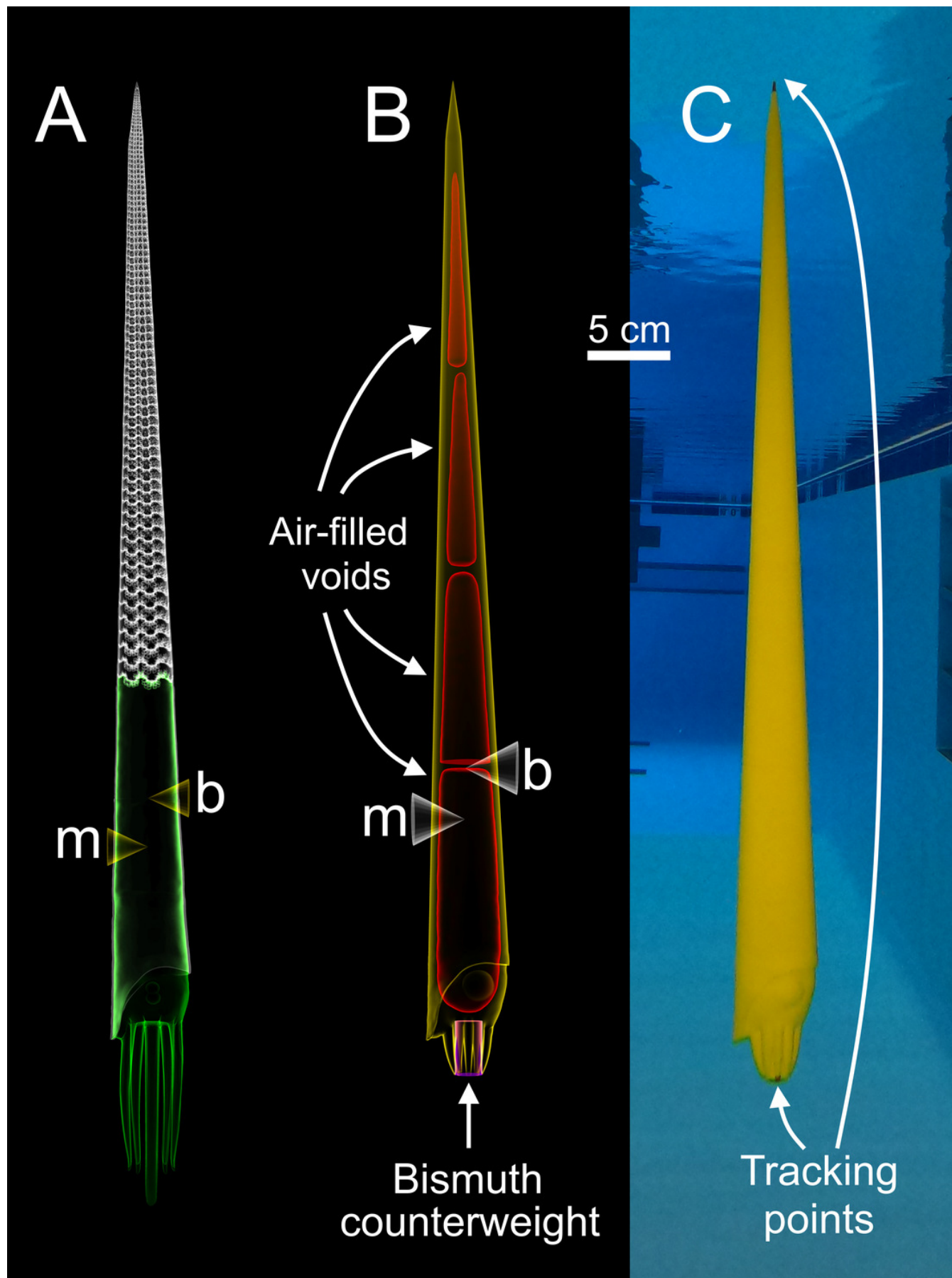
Figure 2

Underwater camera rig used for 3D motion tracking.

A) Schematic of the camera rig relative to the model (yellow) and release mechanism (green). The rig was made strongly negatively buoyant with three steel counterweights at the ends (purple). The wireframe shapes radiating from the cameras denote the approximate field of view. B) Close-up view of waterproof camera and LED light with custom, 3D-printed attachments.

![Underwater camera rig schematic and close-up of waterproof camera and LED light]
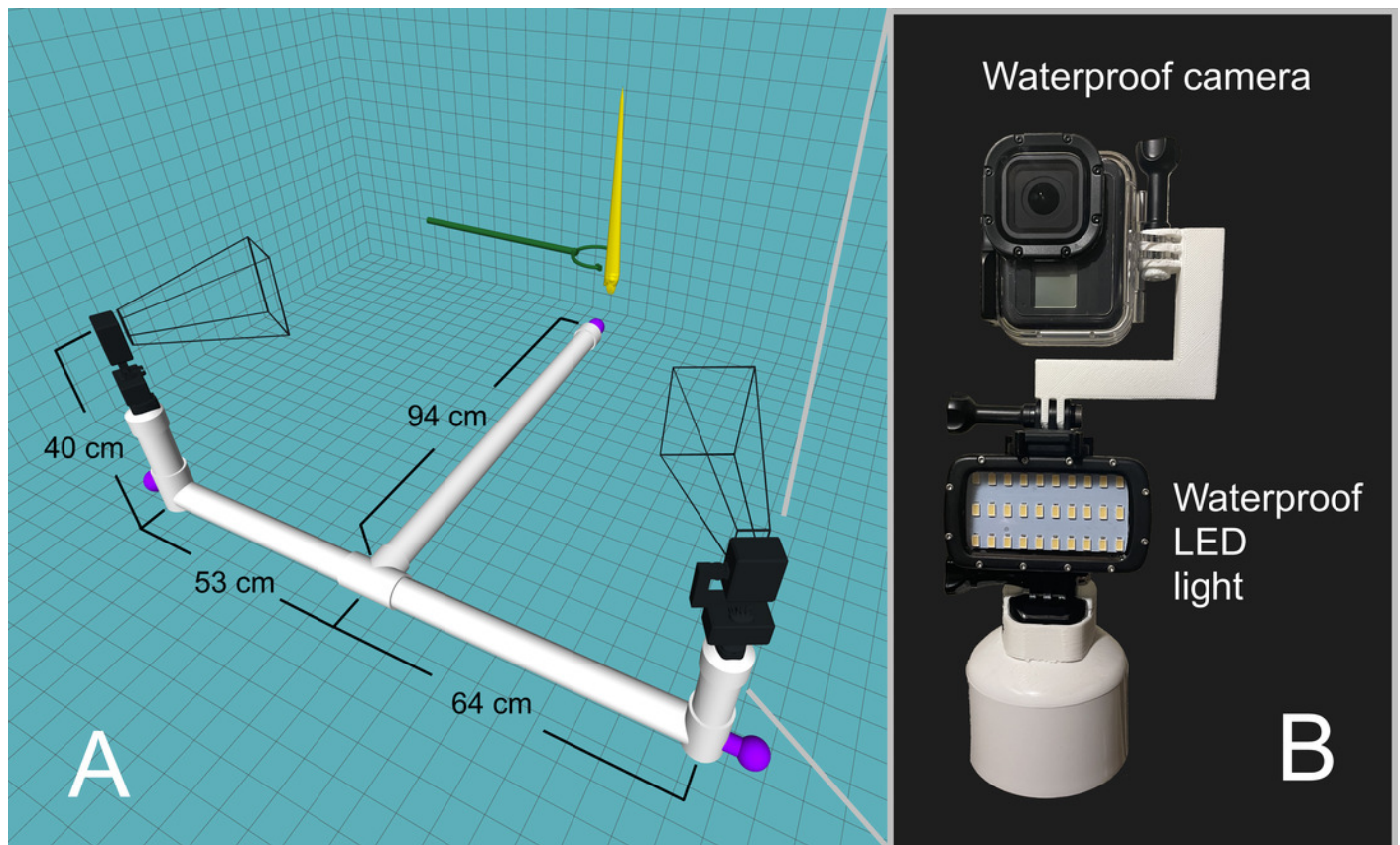
Figure 3

Three-dimensional positions from a common starting point for each model through time.

A) Scenario 1: *Nautilus*-like cruising thrust. B) Scenario 2: *Nautilus*-like cruising thrust scaled by the higher mantle cavity ratio of *Sepia*. C) Scenario 3: *Nautilus*-like peak thrust. D) Scenario 4: slightly negatively buoyant (~0.26% of mass not relieved by buoyancy).
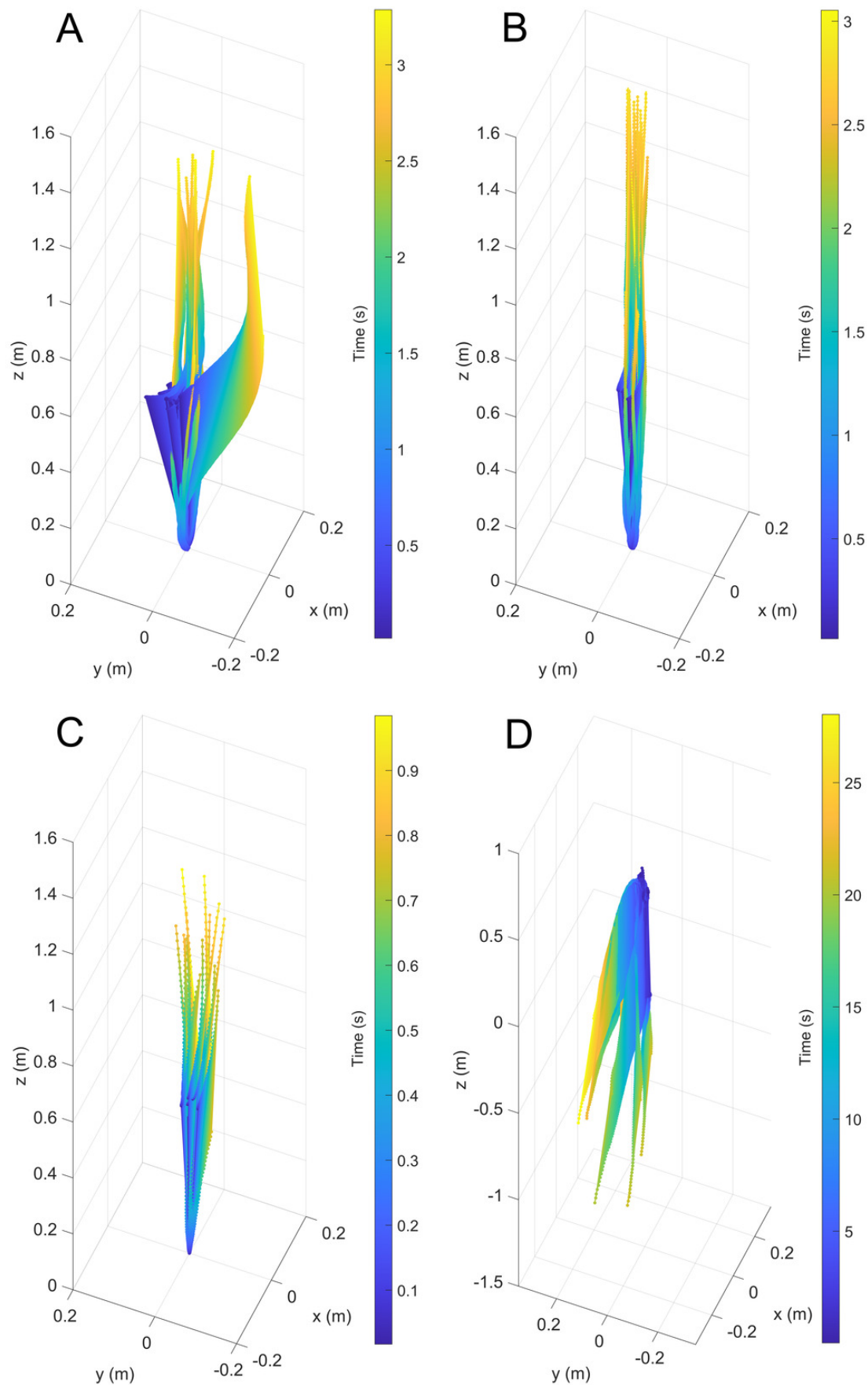
Figure 4

Maximum displacement angle in any direction from the vertical axis through time.

Each trial is distinguished by color. A) Scenario 1: *Nautilus*-like cruising thrust. B) Scenario 2: *Nautilus*-like cruising thrust scaled by the higher mantle cavity ratio of *Sepia*. C) Scenario 3: *Nautilus*-like peak thrust. D) Scenario 4: slightly negatively buoyant (~0.26% of mass not relieved by buoyancy).
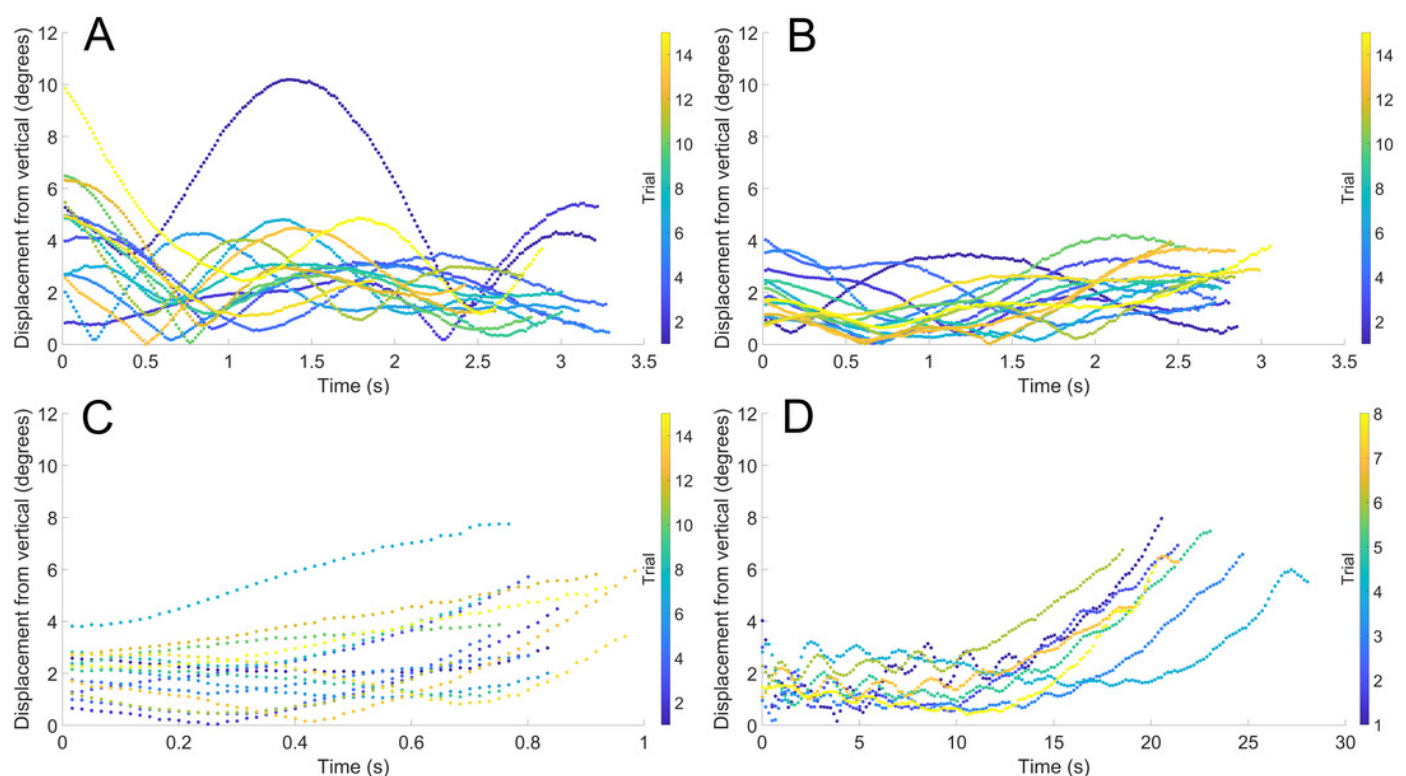
Figure 5

Velocity in the direction of movement as a function of time.

All trials are fit with an asymptote equation. A) Scenario 1: *Nautilus*-like cruising thrust. B)
Scenario 2: *Nautilus*-like cruising thrust scaled by the higher mantle cavity ratio of *Sepia*. C)
Scenario 3: *Nautilus*-like peak thrust. A hydrophobic coating was applied to the original model
to compare the influence of surface texture and friction drag. D) Scenario 4: slightly
negatively buoyant (~0.26% of mass not relieved by buoyancy).
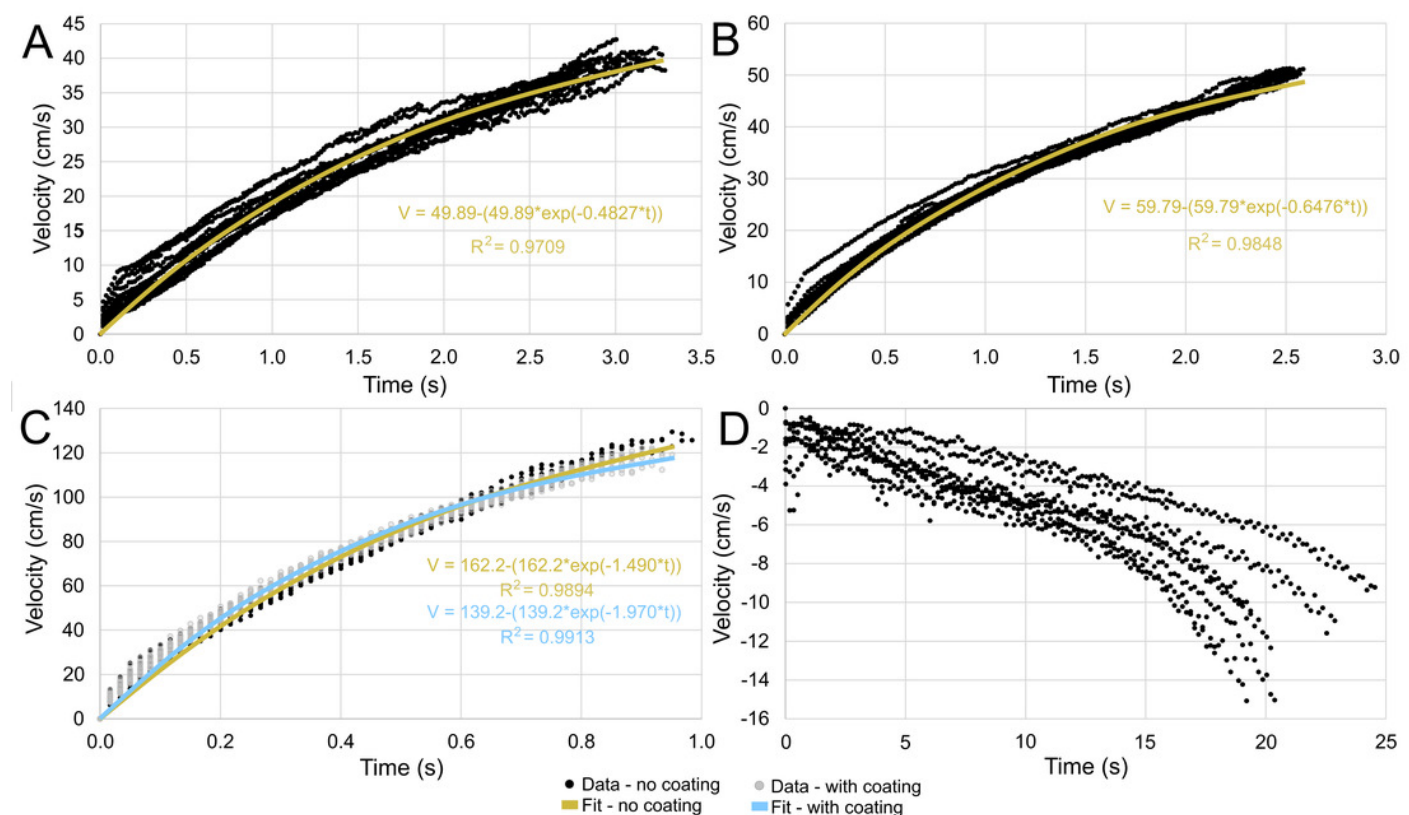
Figure 6

Diagram of vertical predator escape and related terms.

The time required to move one body length (t_{bl}) or half a body length ($t_{bl/2}$) was computed for each velocity profile (V; Fig. 5). This time was multiplied by the velocity of various predators (V_p) to compute the minimum distance required to start jetting (D). A dodge was considered successful if D is less than the length of the predator (L_p). The image of the mosasaur (*Platecarpus*) was created from the outline inferred by *Lindgren et al. (2010)*.
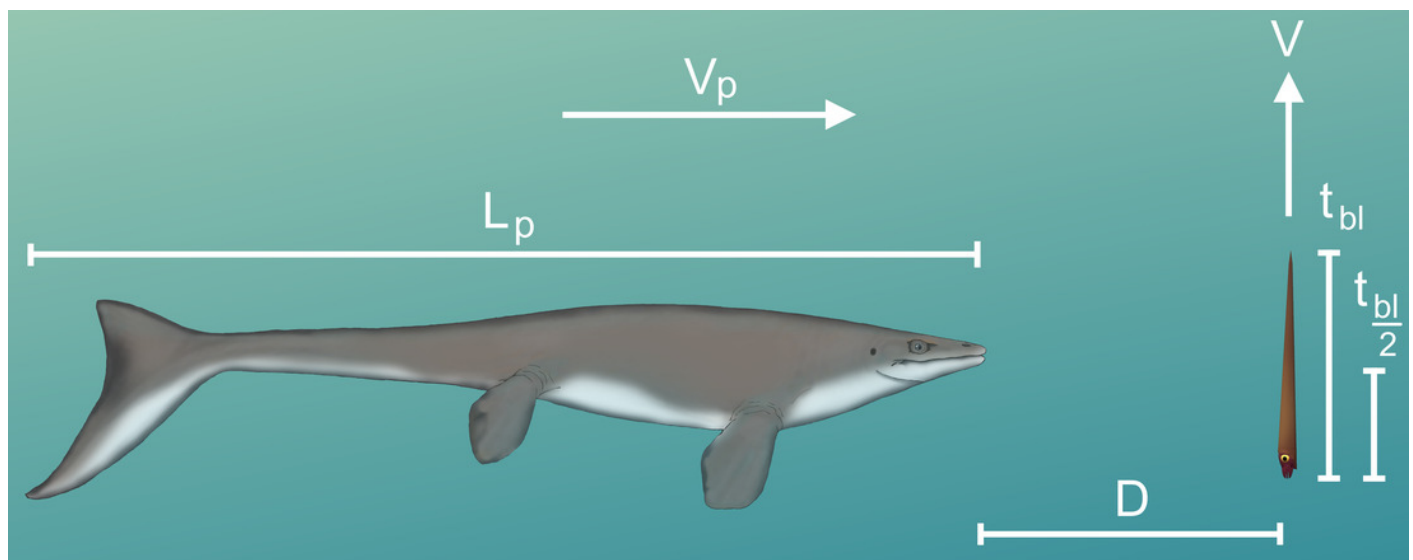
Figure 7

Scenarios involving successful dodging (A) and unsuccessful dodging (B).

The cruising predator first notices the prey (i), then begins to accelerate (ii). After closing in (iii), the predator makes its final lunge for the prey (iv). Cones surrounding the predator indicate hypothetical turning radiuses. For a successful dodge, the orthocone cephalopod must wait until the last possible moment or else the incoming predator could adjust its vertical trajectory. The image of the mosasaur (*Platecarpus*) was created from the outline inferred by *Lindgren et al. (2010)*.
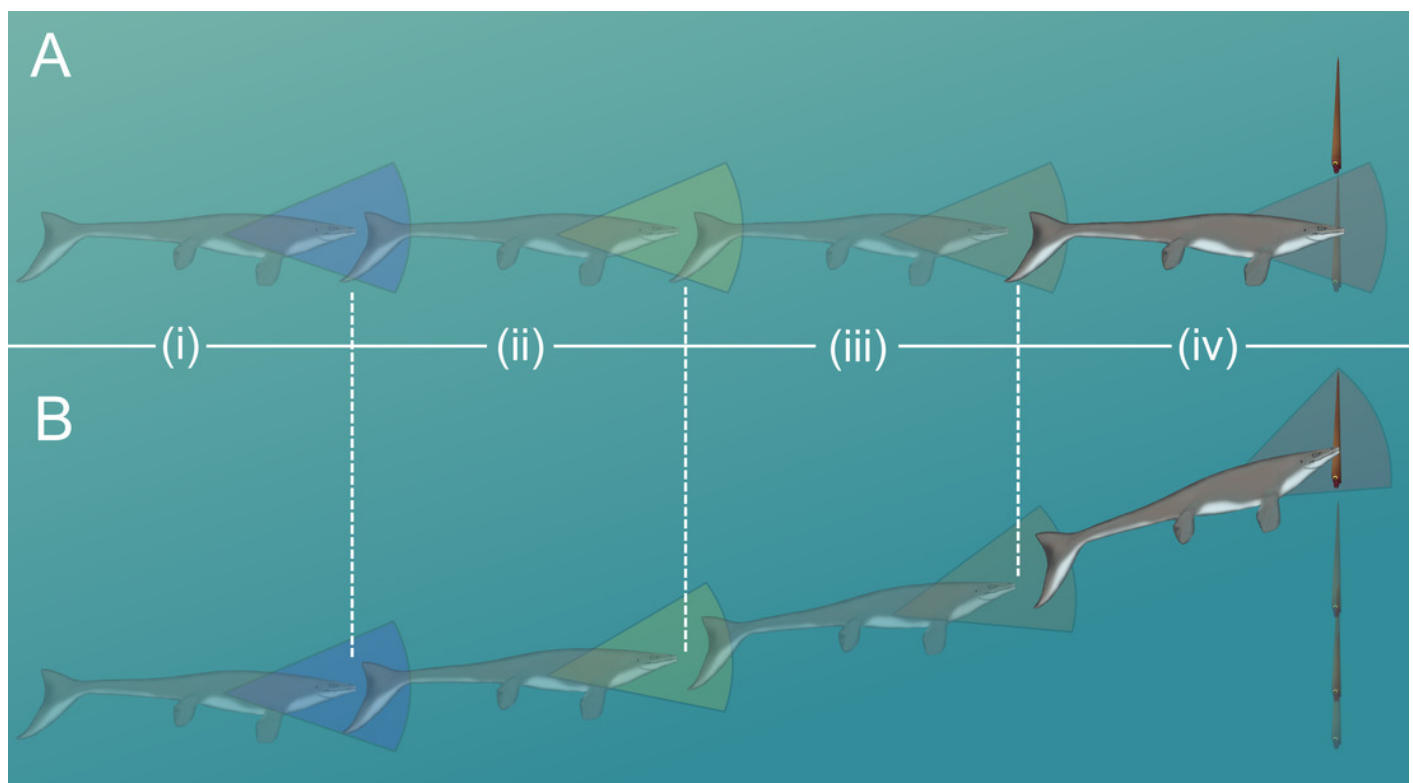
Model centers of mass and buoyancy.

Local centers of mass for the model components (PLA plastic and bismuth counterweight), and total centers of mass and buoyancy for each model (1: *Nautilus*-like cruising thrust; 2: *Nautilus*-like cruising thrust scaled by the higher mantle cavity ratio of *Sepia*; 3: *Nautilus*-like peak thrust; 4: Slightly negatively buoyant). Only the x and z values are reported because the virtual model is perfectly symmetrical. All coordinates are measured relative to the same arbitrary datum (located in the center of the aperture).

Baculite model	PLA x (mm)	PLA z (mm)	Bismuth x (mm)	Bismuth z (mm)	Total center of mass x (mm)	Total center of mass z (mm)	Center of buoyancy x (mm)	Center of buoyancy z (mm)
1	-2.410	130.020	-0.032	-52.279	-1.810	84.070	-1.958	114.191
2	-2.375	119.742	0.439	-57.934	-1.810	84.070	-1.958	114.191
3	-2.052	100.828	0.245	-58.616	-1.810	84.070	-1.958	114.191
4	-1.767	101.472	-2.366	-57.998	-1.810	84.070	-1.958	114.191

Masses (m) and volumes (V) for the virtual and physical model components.

1: *Nautilus*-like cruising thrust; 2: *Nautilus*-like cruising thrust scaled by the higher mantle cavity ratio of *Sepia*; 3: *Nautilus*-like peak thrust; 4: Slightly negatively buoyant. PLA = 3D printed plastic; Bi = bismuth counterweight; wd = water displaced; Mass def. = mass deficiency required to impart the computed buoyant forces (Table 3); glue = the cyanoacrylate glue used to secure each counterweight. The residual mass in the negatively buoyant experiment (denoted with *) was not weighed, but rather its volume was inserted into the model with a syringe (~0.5 cm^3).

Baculite model	Virtual							Physical					
	V_{PLA} (cm³)	m_{PLA} (g)	V_{Bi} (cm³)	m_{Bi} (g)	m_{wd} (g)	m_{total} (g)	Mass def. (g)	m_{PLA} (g)	m_{Bi} (g)	m_{glue} (g)	m_{wd} (g)	m_{total} (g)	Mass def. (g)
1	124.319	155.275	5.651	52.490	212.209	207.765	4.444	157.875	49.737	0.101	212.209	207.713	4.496
2	130.978	163.592	4.437	41.211	212.209	204.803	7.406	162.205	42.518	0.207	212.209	204.930	7.280
3	126.935	158.542	2.018	18.745	212.209	177.287	34.922	158.529	18.612	0.355	212.209	177.496	34.713
4	152.102	189.975	2.453	22.789	212.209	212.764	-0.555	187.063	24.875	0.206	212.209	212.144	-0.5*

Virtual and actual hydrostatic stabilities (S_t) and thrusts (F), and computed percent errors.

1: *Nautilus*-like cruising thrust; 2: *Nautilus*-like cruising thrust scaled by the higher mantle cavity ratio of *Sepia*; 3: *Nautilus*-like peak thrust; 4: Slightly negatively buoyant.

Baculite model	Virtual S_t	Actual S_t	St error (%)	Target F (N)	Actual F (N)	Thrust error (%)
1	0.505	0.492	-2.57	0.0436	0.0441	1.17
2	0.505	0.499	-1.19	0.0727	0.0714	-1.77
3	0.505	0.483	-4.36	0.3426	0.3405	-0.60
4	0.505	0.454	-10.10	-0.0054	-0.0049	-9.42

Velocities, travel times, and asymptote equation coefficients.

Uncertainty reflects bounds of 95% confidence intervals. The asymptotic velocity (in cm/s) is predicted by coefficient "a" of Equation 6. Coefficient "b" governs the slope. The maximum body lengths per second (Max. bl/s) were computed by dividing velocity by the body length of the models (57 cm). The time required to move one body length (t_{bl}) and half of one body length ($t_{bl/2}$) was computed for each model (1: *Nautilus*-like cruising thrust; 2: *Nautilus*-like cruising thrust scaled by the higher mantle cavity ratio of *Sepia*; 3: *Nautilus*-like peak thrust, coated and uncoated with hydrophobic silicone spray).

Model	a (V asymptote cm/s)	b	Max. bl/s	t_{bl} (s)	$t_{bl/2}$ (s)
1	49.89 ± 0.72	0.4827 ± 0.0116	0.875 ± 0.013	2.633 ± 0.048	1.755 ± 0.032
2	59.79 ± 0.58	0.6476 ± 0.0111	1.049 ± 0.010	2.101 ± 0.026	1.395 ± 0.018
3 (uncoated)	162.2 ± 3.10	1.490 ± 0.045	2.846 ± 0.054	0.826 ± 0.019	0.552 ± 0.013
3 (coated)	139.2 ± 1.50	1.970 ± 0.040	2.442 ± 0.026	0.815 ± 0.012	0.535 ± 0.008

Predator evasion potential of orthocone cephalopods using mostly extant predators as analogues.

Dodges are considered successful (bold numbers) when the minimum distance required to start jetting (D) is less than the body length of a predator (L_p) moving at some incident velocity (V_p). The subscripts in D values refer to different thrust scenarios in the models (1: *Nautilus*-like cruising thrust; 2: *Nautilus*-like cruising thrust scaled by the higher mantle cavity ratio of *Sepia*; 3uc: *Nautilus*-like peak thrust with no coating; 3c: *Nautilus*-like peak thrust, coated in hydrophobic silicone spray). The velocity of *Platecarpus* (denoted by *) is only an estimate of metabolically optimal velocity (*Motani, 2002*), therefore critical/lunge velocity should be much higher.

Species	Common name	L_p (m)	V_p (m/s)	Reference	Moving one body length (57 cm)				Moving 1/2 body length (28.5 cm)			
					D_1 (m)	D_2 (m)	D_{3uc} (m)	D_{3c} (m)	D_1 (m)	D_2 (m)	D_{3uc} (m)	D_{3c} (m)
Platecarpus	Mosasaur	4	0.38*	Motani, 2002	**1.00**	**0.80**	**0.31**	**0.31**	**0.67**	**0.53**	**0.21**	**0.20**
Megaptera novaeangliae	Humpback whale	12.7	5	Segre et al., 2020	13.17	**10.51**	**4.13**	**4.08**	**8.78**	**6.98**	**2.76**	**2.68**
Crocodylus porosus	Saltwater crocodile	5	8	Benga et al., 2010	21.06	16.81	6.61	6.52	14.04	11.16	**4.42**	**4.28**
Delphinus delphis	Short-beaked common dolphin	1.8	8	Tanaka et al., 2019	21.06	16.81	6.61	6.52	14.04	11.16	4.42	4.28
Stenella attenuata	Pantropical spotted dolphin	1.86	11	Tanaka et al., 2019	28.96	23.11	9.09	8.97	19.31	15.35	6.07	5.89
Isurus oxyrincus	Shortfin mako shark	2.1	19	Fernandez-Waid et al., 2019	50.03	39.92	15.69	15.49	33.35	26.51	10.49	10.17